# Martin Marietta Laboratories

MARTIN MARIETTA
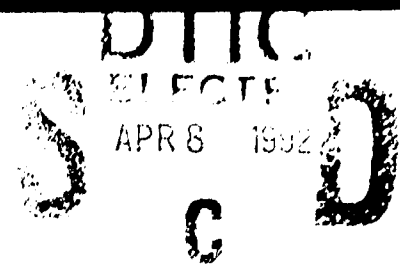
MML TR 92-13c

A Study of the Influence of Alloying Additions on the Passivity of Aluminum

Annual Report

December 1, 1990 - November 30, 1991

Submitted to:

Submitted by:

G.D. Davis and B.J. Rees
Martin Marietta Laboratories, Baltimore, MD 21227

B.A. Shaw and M. Ferry
The Pennsylvania State University, State College, PA 16802

March 1992
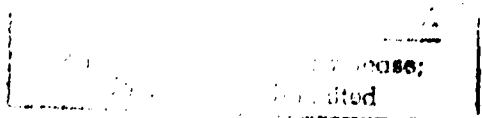
92 4 07 100

92-09027

REPORT DOCUMENTATION PAGE

Form Approved
OMB No. 0704-0188

1a. REPORT SECURITY CLASSIFICATION Unclassified	1b. RESTRICTIVE MARKINGS None
2a. SECURITY CLASSIFICATION AUTHORITY	3. DISTRIBUTION/AVAILABILITY OF REPORT
2b. DECLASSIFICATION/DOWNGRADING SCHEDULE None	Unlimited

4. PERFORMING ORGANIZATION REPORT NUMBER(S) MML TR 91-10c	5. MONITORING ORGANIZATION REPORT NUMBER(S)

6a. NAME OF PERFORMING ORGANIZATION Martin Marietta Corporation Martin Marietta Laboratories	6b. OFFICE SYMBOL (If applicable) MML	7a. NAME OF MONITORING ORGANIZATION Defense Contract Administration Services Management Area - Baltimore
6c. ADDRESS (City, State, and ZIP Code) 1450 South Rolling Road Baltimore, Maryland 21227-3898		7b. ADDRESS (City, State, and ZIP Code) 300 East Joppa Road Baltimore, Maryland 21204-3099

8a. NAME OF FUNDING/SPONSORING ORGANIZATION Office of Naval Research	8b. OFFICE SYMBOL (If applicable) ONR	9. PROCUREMENT INSTRUMENT IDENTIFICATION NUMBER N00014-85-C-0638

| 8c. ADDRESS (City, State, and ZIP Code) 800 North Quincy Street Arlington, VA 22217-5000 | 10. SOURCE OF FUNDING NUMBERS |

PROGRAM ELEMENT NO.	PROJECT NO.	TASK NO.	WORK UNIT ACCESSION NO.

11. TITLE (Include Security Classification)

A Study of the Influence of Alloying Additions on the Passivity of Aluminum

12. PERSONAL AUTHOR(S)

G.D. Davis, B.J. Rees, B.A. Shaw and M. Perry

13a. TYPE OF REPORT Annual	13b. TIME COVERED FROM 12/1/90 TO 11/30/91	14. DATE OF REPORT (Year, Month, Day) March 31, 1992	15. PAGE COUNT 55

16. SUPPLEMENTARY NOTATION

17. COSATI CODES			18. SUBJECT TERMS (Continue on reverse if necessary and identify by block number)
FIELD	GROUP	SUB-GROUP	Approved for public release; distribution unlimited. Reproduction in whole or in part is permitted for any purpose of the United States Government.

19. ABSTRACT (Continue on reverse if necessary and identify by block number)

The corrosion behavior of nonequilibrium AlTa and AlW alloys produced by either dynamic compaction or sputter deposition has been evaluated. Dynamically compacted material showed no enhanced passivity as a result of precipitates formed during powder formation. No new precipitates were found that originated during the dynamic compaction process when water was used to reflect the shock wave. Sputter-deposited AlW and AlTa alloys exhibited considerable enhanced resistance to pitting corrosion over a range of pH's extending from pH 9.6 to pH 0. Surface analysis showed that although very little oxidized W is found in the passive film at near-neutral pH's, the passive film at pH3 consists of comparable amounts of oxidized W and Al. A review of the different mechanisms that have been proposed to explain the passivity of this class of alloys suggests that the pitting resistance of Al-W is likely to result from a repassivation of metastable pits due to the stability of oxidized W in low-pH environments.

20. DISTRIBUTION/AVAILABILITY OF ABSTRACT ☐ UNCLASSIFIED/UNLIMITED ☐ SAME AS RPT ☐ DTIC USERS	21. ABSTRACT SECURITY CLASSIFICATION Unclassified
22a. NAME OF RESPONSIBLE INDIVIDUAL Dr. Guy D. Davis	22b. TELEPHONE (Include Area Code) 410-247-0700 x2376	22c. OFFICE SYMBOL

DD Form 1473, JUN 86   Previous editions are obsolete.   SECURITY CLASSIFICATION OF THIS PAGE

TABLE OF CONTENTS

Accession For

NTIS GRA&I

DTIC TAB

Unannounced

Justification

By

Distribution/

Availability Codes

Avail and/or

Dist   Special

A-1

ii

LIST OF FIGURES

LIST OF FIGURES

LIST OF FIGURES

EXECUTIVE SUMMARY

The corrosion behavior of nonequilibrium AlTa and AlW alloys produced by either dynamic compaction or sputter deposition has been evaluated. Dynamically compacted material showed no enhanced passivity as a result of precipitates formed during powder formation. No new precipitates were found that originated during the dynamic compaction process when water was used to reflect the shock wave. Sputter-deposited AlW and AlTa alloys exhibited considerable enhanced resistance to pitting corrosion over a range of pH's extending from pH 9.6 to pH 0. Surface analysis showed that although very little oxidized W is found in the passive film at near-neutral pH's, the passive film at pH 3 consists of comparable amounts of oxidized W and Al. A review of the different mechanisms that have been proposed to explain the passivity of this class of alloys suggests that the pitting resistance of Al-W is likely to result from a repassivation of metastable pits due to the stability of oxidized W in low-pH environments.

INTRODUCTION

Aluminum and its conventional alloys are susceptible to localized attack in chloride-containing environments. Although the corrosion resistance of steels can be dramatically improved by the incorporation of chromium, molybdenum, and other elements to make stainless steels, there are no equivalent conventional stainless aluminum alloys. The failure to produce such alloys is largely due to the very low solubility of passivating species in aluminum; above a small fraction of an atomic percent, these species form precipitates and the microgalvanic couples between the two phases leads to enhanced corrosion.

In the last several years, supersaturated aluminum alloys with Mo, Cr, Ta, W, Zr, Nb, Zn, V, Cu, Ti, and Si have been produced by several groups using rapid solidification or other nonequilibrium methods.[1-22] Several of these alloys have shown significant improvements in passivity in chloride-containing environments. For our sputter-deposited thin films, Al-Ta and Al-W alloys have shown the best performance with pitting potentials well above 0 mV (SCE) and passive regions exceeding 1000 mV.[4,5,7,8]

During this contract year, we have pursued two areas of investigation: production and testing of bulk material and continued investigation of the mechanisms by which these stainless aluminum alloys exhibit enhanced passivity. Although thin films of stainless aluminum have potential applications as cladding material and in electronic devices, bulk material has many more possible uses. Accordingly, we have characterized and evaluated the corrosion performance of material produced by dynamic compaction of rapidly solidified (RS) powders.

Several different mechanisms have been proposed to explain the passivity of stainless aluminum alloys, including electrostatic repulsion of Cl^- by oxidized solute atoms,[1-3] formation of an oxidized solute barrier layer,[3,4] stabilization of the passive film oxide structure,[6] reduction in Cl^- adsorption due to pH_{pzc} changes,[12-16] increased competition among possible Cl^- adsorption sites due to disordered oxide films above the grain boundaries of small-grained material,[21,22] stabilization of occluded cells by low-pH-stable solute oxides,[21,22] and replacement of oxidized Al in the passive film by oxidized solute to form a more stable oxide.[19,20] Additionally, Urquidi and Macdonald[23] have proposed a solute-vacancy interaction model (SVIM)

in which it is suggested that pits originate as vacancies collect at the metal/passive film interface, which causes the film to collapse locally; highly oxidized solute atoms form complexes with cation vacancies formed by Cl⁻ adsorption to reduce the diffusivity of the vacancies and slow their buildup at the metal/film interface.

It is very possible that more than one mechanism controls the passivity of the various stainless aluminum alloys under different conditions. To further evaluate the mechanisms governing the passivity of these alloys, especially Al-W and Al-Ta, which have shown the best corrosion performance, we have continued to characterize and test these alloys under different conditions. Specifically, we have examined the electrochemical behavior and, in some cases, the surface chemistry of Al-W and Al-Ta alloys in KCl solutions of different pH's and different Cl⁻ concentrations. We have also examined their behavior in artificial seawater for the obvious technological interests and to augment the mechanistic investigations in KCl.

The behavior of these alloys at non-neutral pH values is of special interest since the Pourbaix diagrams for W and Ta and the literature for stainless steels suggest that it would be possible to extend the passivity of Al outside the range of 4 to 9 through the nonequilibrium addition to these elements to Al. Pourbaix diagrams for Al and W are shown in Fig. 1[24]. This figure reveals that passivity is anticipated at low pH for W values and at neutral pH values for Al. It is reasonable to believe that the passivity of Al could be extended to lower pH values through the nonequilibrium addition of W. Indeed, the literature for stainless steels [25-28] has shown that the addition of W (in the presence of a significant amount of Ni) enhances passivity at low pH values. Similarly, a comparison of the Pourbaix diagrams for Al and Ta (Fig. 2) suggests that Al passivity could be extended to both high and low pH ranges with the nonequilibrium addition of Ta.

As a type of control, we have also examined the electrochemical behavior and surface chemistry of an Al-Au alloy whose passive film should consist solely of aluminum oxides/hydroxides without oxidized solute. We then compare these results, along with microstructural characterization, with predictions from many of the different proposed mechanisms.

3
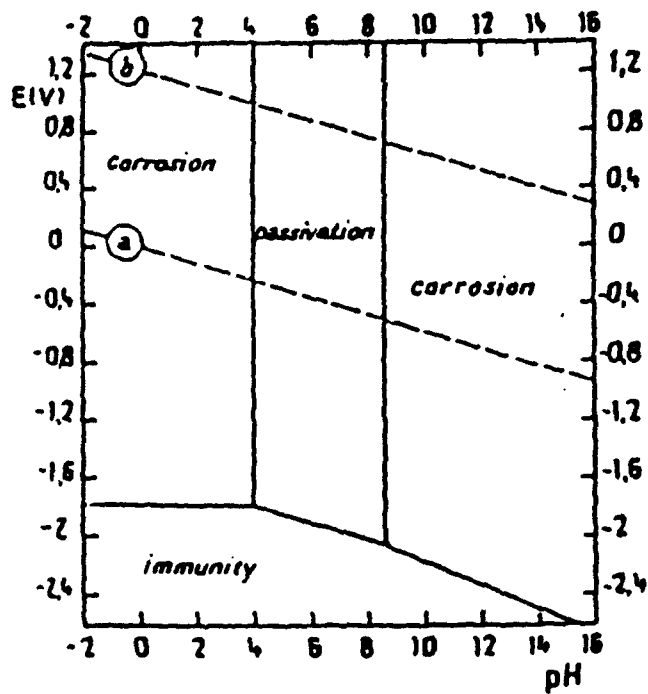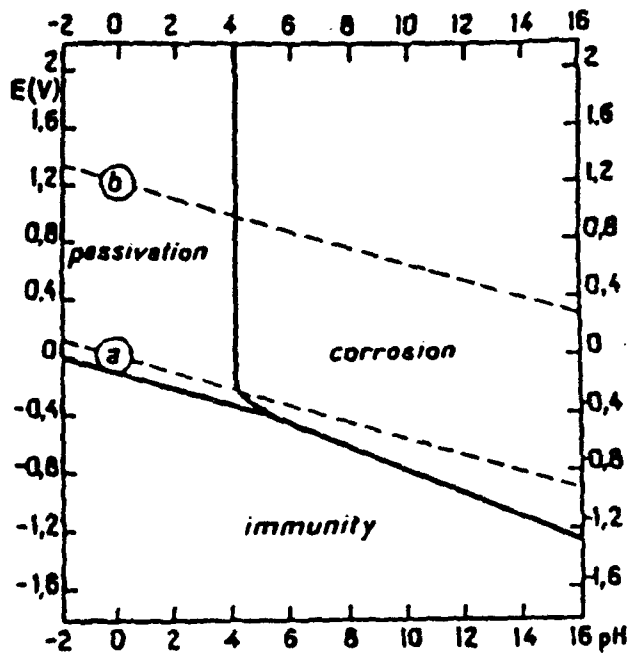
Figure 1   Pourbaix diagrams for a) Al and b) W (from Reference 32).
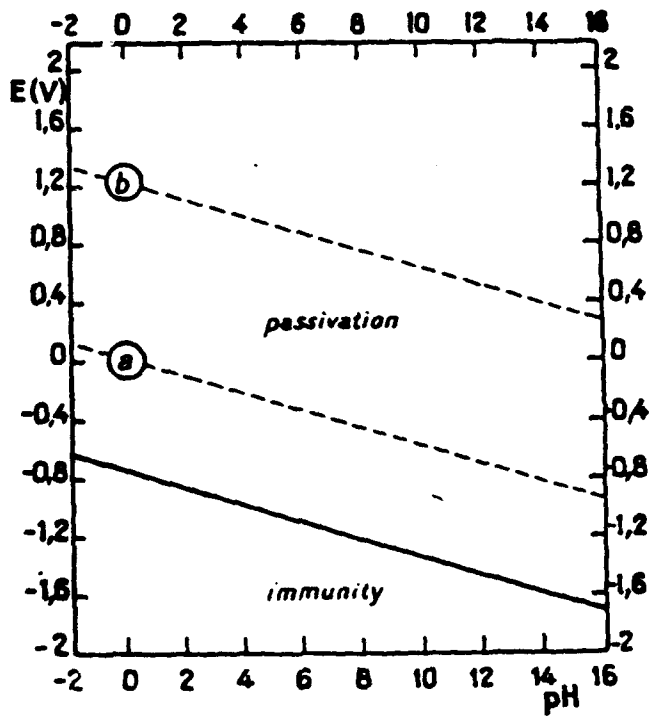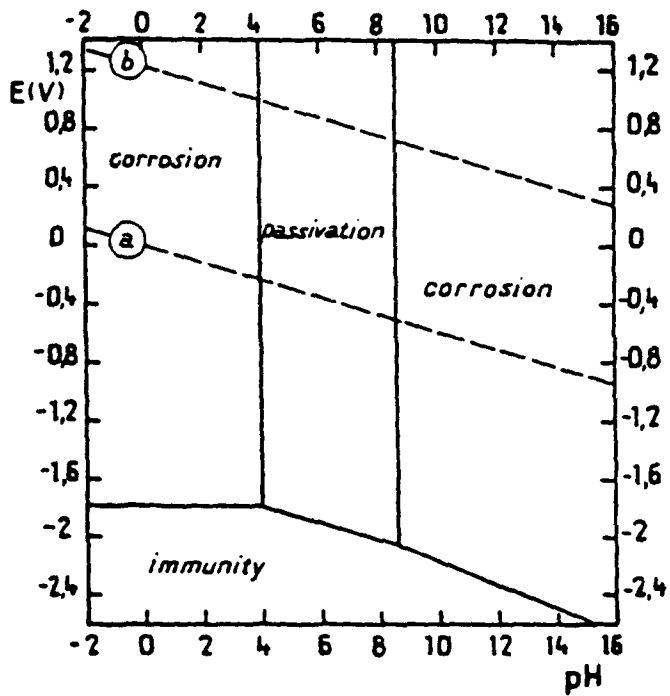
Figure 2   Pourbaix diagrams for a) Al and b) Ta (from Reference 32).

5

EXPERIMENTAL PROCEDURE

Bulk Alloy Production

Bulk alloys were prepared by dynamically consolidating RS aluminum alloy powders. Two batches of RS powders were produced by Valimet, Inc. Details concerning the atomization of the powders were presented in last year's report.[29] The compositions for the two batches of powder are listed in Table 1.

TABLE 1. RS Powders Produced at Valimet Inc.

Batch #	Composition	Produced	Presence of precipitates by	
			XRD[a]	SEM[b]
1	Al-0.56W[c]	May 1990	yes	yes
	Al-0.32Ta		no	yes
	pure Al			
2	Al -0.85W	Nov. 1990	yes	yes
	Al-1.0Ta		yes	----

[a] X-ray Diffraction
[b] Scanning Electron Microscopy
[c] Al - 0.56 at.%W

Dynamic consolidation of the RS powders was performed at Idaho National Engineering Laboratories (INEL) in the winter and spring of 1991. This process utilizes shock waves, generated by explosives, to cause interparticle melting and bonding. Dynamic consolidation and the conventional powder consolidation method, hot isostatic pressing (HIP'ing), can be compared in Fig. 3. Because dynamic consolidation yields only moderate increases in temperature for periods of several microseconds and, therefore, should not encourage precipitation of a second phase, it was chosen over HIP'ing. Schematics of the two dynamic consolidation processes employed to produce our bulk alloys are presented in Fig. 4. In both setups the RS powders were placed in a 6061 aluminum tube. Explosives were used to crush another 6061 Al tube against the one containing the RS powders - which results in the propagation of a

CONVENTIONAL METHOD
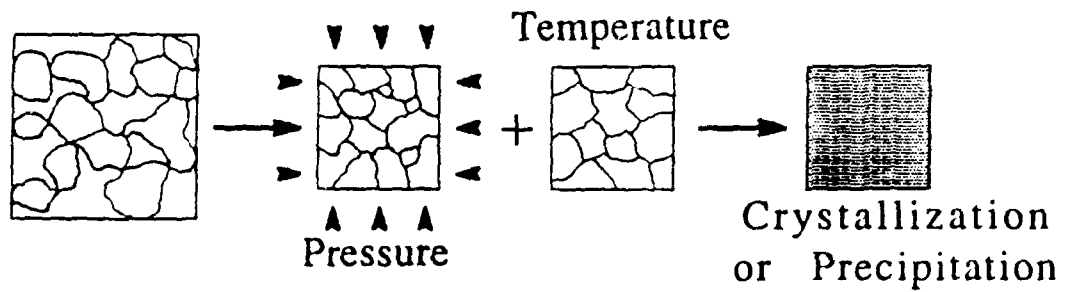
DYNAMIC COMPACTION
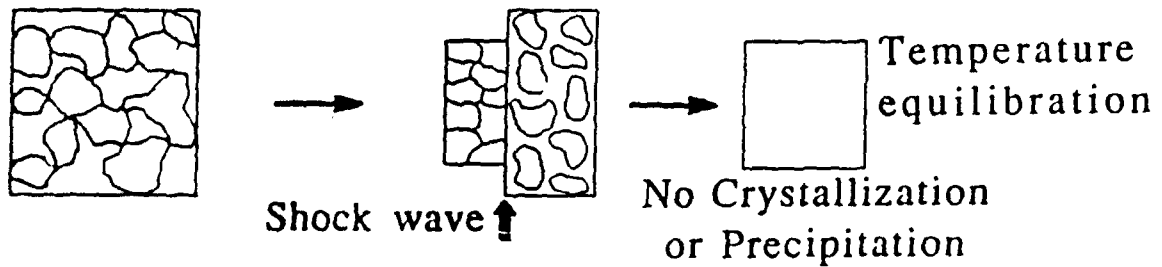
Figure 3   The conventional method for powder consolidation (Hot Isostatic Pressing) vs dynamic compaction.
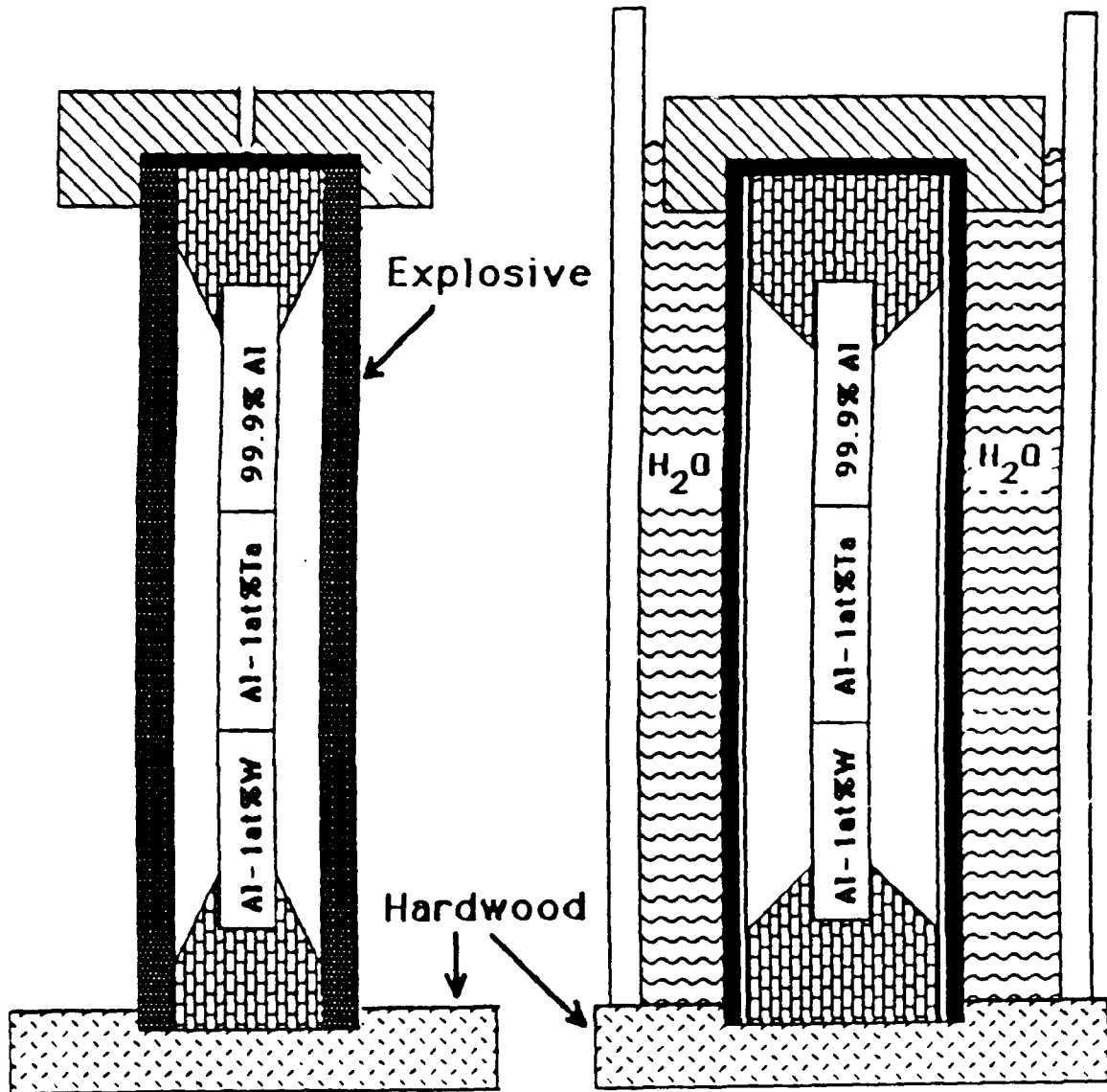
Figure 4   Schematic representation of INEL dynamic consolidation processes a)
            without water and b) with water.

shock wave through the powder. The first method, without the water surrounding the explosive, produces a shock wave with a velocity of approximately 3.6 km/s. The second method, with the water surrounding the explosive, requires much less explosive because of the reflection from the water and produces a faster shock wave with a velocity of approximately 7 km/s. Additonal details concerning the dynamic consolidation process can be found in References 30 and 31. The powders for our investigation were consolidated under the conditions described in Table 2. The presence of precipitates in these powders was confirmed by either XRD, SEM or both. The explosive consolidations were performed at INEL's remote testing grounds approximately 50 miles east of Idaho Falls. A photograph of the explosion and the adjacent bunker at this facility is presented in Fig. 5.

TABLE 2 Dynamically Compacted Material Produced by INEL

Shot #	Material	Condition	Powder Size (μm)
239	Al	air	75-150
	Al-0.85W	"	"
	Al-1Ta	"	"
240	Al	water	75-150
	Al-0.85W	"	"
	Al-1Ta	"	"
241	Al	water	75-150
	Al-0.85W	"	"
	Al-1Ta	"	20-50
242	Al	air	75-150
	Al-0.85W	"	"
	Al-1Ta	"	"
243	Al	air	75-150
244	Al-0.3Ta	air	75-150
245	Al-0.85W	air	20-50

Figure 5.   Photograph of the dynamic compaction operation.

Thin-film Production

One-micron-thick alloy films were produced by RF magnetron sputter deposition (identical alloyed targets) or co-sputter deposition (one target Al -- the other W) onto Si single-crystal wafers 2-in. in diameter (5.08 cm). The co-sputter deposition process has been described elsewhere.[1-5] Briefly, it involves the use of two different target materials with the solute sputtered at a lower power level, typically between 15 and 40 watts, and the Al sputtered at a higher power of approximately 360 watts. Other low W concentration alloys were sputtered to a thickness of 2 microns using two alloyed targets with both of the sputtering guns set at a power level of 400 watts. This process provides uniformity of alloy composition over the surface of the wafer. In a few cases, alloy films were produced using alloyed targets of Al-1%W and Al-5%W. This procedure produced intermediate composition alloys with only slight variation across the wafer. The Si substrates were kept at 77 K for these deposition processes. A few specimens were produced by co-sputter deposition onto a rotating substrate holder to alleviate concentration gradients. These specimens were deposited at ambient temperatures. Solute concentrations for the alloys were determined by induction coupled plasma (ICP); all concentrations are given in at.%. After deposition, the 2-in.-dia. wafers were cleaved into 16 smaller specimens for further evaluation.

Electron Microscopy and X-ray Diffraction

High-resolution scanning electron microscopy (HSEM) and transmission electron microscopy (TEM) of the as-sputtered surfaces were performed on a JEOL 100 CX at 40 keV and 100 keV, respectively. The specimens were evaluated in the as-produced condition, i.e., without a thin coating of C or Pt sputtered on top of the alloy film, to ascertain grain morphology and size. Specimens were prepared for TEM by polishing the back side of the silicon until the final thickness of the wafer was close to 50 μm. A copper-rhodium mask with an oval hole was then glued to the polished silicon side with epoxy. An area thin enough for transmission of the electron beam was made by ion milling the Si side with argon using a Gatan Model 600 ion miller. The sample was ion milled on a cold stage to prevent heating during thinning.

Glancing angle x-ray diffraction (GXRD),[32] with a constant angle of 10 degrees between the incident x-ray beam and the film surface, was used to check the thin-film alloys for precipitate formation. Diffraction of compacted material was performed at

both glancing and normal incidence. The experiments were performed on a Scintag diffractometer using a monochromatic Cu Kα x-ray source. The glancing angle was chosen to both optimize the signal from the metal film and prevent diffraction from the Si single crystal.

Electrochemical Experiments

Thin-film alloys

Individual electrochemical specimens were prepared by attaching a coated lead wire, and masking the back and edges of the specimens with a marine epoxy paint. Anodic potentiodynamic polarization curves were generated at a scan rate of 0.2 mV/s at ambient room temperature (23 to 27°C). A limited number of experiments were also run at a rate of 0.02 mV/s. All of the experiments were conducted on at least duplicate specimens in aerated chloride solutions with pH values ranging from 0 to 9.6 for the Al-W alloys and 3 to 12 for the Al-Ta alloys. After immersion and prior to polarization, the open-circuit potentials, E_{oc}, were allowed to stabilize for at least 1 hour. All potentials given in this report are relative to a saturated calomel reference.

Bulk alloys

The dynamically consolidated bulk metals and the control materials (5086 Al, pure W, and pure Ta) were tested under the same electrochemical conditions as described for the thin-film alloys. Prior to testing, the bulk materials were wet ground to a 600 grit finish and rinsed in methanol and deionized water. The specimens were tested in a flat cell (EG&G flat-cell model K0235) which simplified mounting of the specimens since no lead wire attachment or coating of the specimens were required. Because of the poor performance of the dynamically compacted alloys at neutral pH, no experiments were conducted on these materials at either high or low pH.

Surface Analysis

The chemistry of the Al-W passive film in pH 3 solutions was investigated in the as-sputtered condition, at the open circuit potential, and at various potentials up to E_p. The same specimens were repeatedly used to prevent compositional variations across the wafer (and hence from sample to sample) from affecting the results. Details

of the procedure have been reported previously.[3,4] Changes in the surface chemistry induced by the transfer procedure and by exposure to ultrahigh vacuum have been examined and possible artifacts were shown to be either small (e.g., additional oxidation) or tractable (e.g., adventitious contamination), and the differences in the measured surface chemistry were shown to originate in the electrolyte.[2,33]

The XPS measurements were made using a Surface Science Instruments Model SSX 100-03 spectrometer with a monochromatized Al Kα x-ray source and a hemispherical electron energy analyzer with multichannel detection. The x-ray source was focused to a spot size of 600 μm and the surface charge was neutralized with low-energy electrons. Binding energies were normalized to that of adventitious hydrocarbon at 284.8 eV. Survey spectra provided a qualitative analysis of the surface, whereas high-resolution spectra [with a full width at half maximum (FWHM) of the Au $4f_{7/2}$ peak of 1.1 eV] of the O 1s, C 1s, Al 2p, and W 4f photoelectron peaks were used for quantitative analysis and chemical state determination. Quantitative analysis data were obtained using peak areas and sensitivity factors determined from standards with our spectrometer. Chemical state separation was achieved by curve fitting, the details of which are presented in Reference 3, with the W 4f doublet being constrained with a peak separation of 2.2 eV and an area ratio of 1.33. Chemical state assignments were made using the National Institute of Standards and Technology (NIST) data base,[34] supplemented with other sources.[35-41]

Sputter-depth profiling was achieved using 4 keV Ar$^+$ ions from a Perkin-Elmer differentially pumped ion gun. The x-ray source was focussed to 300 μm and data acquired during periods of no ion bombardment using survey-spectra resolution in an unscanned mode. Sputter rates were approximated using Ta_2O_5 specimens with known oxide thicknesses.

RESULTS AND DISCUSSION

Dynamically Consolidated Materials

X-ray diffraction and SEM of the RS Al-Ta and Al-W powders revealed precipitates in both sets of the powders. Those observed near the surface of the RS powders were on the order of 1 micron in size and different characteristic shapes were noted for the precipitates in each alloy. (Larger precipitates may have been present in the interior of

the particles, especially for the 75- to 150-μm particles.) Figure 6 shows SEM micrographs of the Al-Ta and Al-W powders. The micrograph for the Al-Ta powders show both a secondary electron image and a backscattered image, which highlights compositional variations (high Z elements show up brighter). The Ta-rich areas are also visible in the secondary electron image; both images reveal a dendritic shape for the precipitate. X-ray diffraction of the Al-Ta RS powders, Fig. 7, confirmed that the precipitate in the Al-Ta alloy was $TaAl_3$ (the low-solute-concentration precipitate predicted by the binary phase diagram). X-ray diffraction of the compacted Al-Ta material revealed that no other types of precipitates formed during the explosive consolidation process. The precipitates observed in the Al-W powders were more acicular in shape. An XRD spectrum for the Al-W 75- to 150-μm powder is presented in Fig. 8. Unidentifiable peaks not corresponding to Al, WAl_{12}, or Al_5W were found at d values of 4.697 (2θ ~19°) and 3.307 (θ ~27°). X-ray diffraction spectra after compaction, using air and water as shown in Fig. 4, are presented in Fig. 9. The alloy compacted using water shows a peak at a d value of 4.697, the same unidentified peak that was observed prior to consolidation, whereas the alloy compacted in air contains a precipitate identified as WAl_{12} (the low-solute γ-phase precipitate predicted by the binary phase diagram). The precipitates in the Al-W air-compaction most likely resulted from the lower shock wave velocity and longer heating time associated with the air technique. The material from shots 239 (Al and Al-Ta), 240 (Al and Al-Ta), 242, 243, 244 and 245 was fully consolidated with no cracks or prominent voids observed.

Anodic polarization behavior for the dynamically consolidated alloys from shot 242 are shown in Figs. 10 and 11. Identical polarization behavior was observed for the alloys produced in shots 243, 244 and 245. No passivity was observed for any of the dynamically consolidated alloys, which is essentially identical to that of dynamically compacted unalloyed Al (Fig. 11). SEM micrographs of the specimens after testing, Fig. 12, reveal that the precipitates led to the formation of microgalvanic cells and pitting. Fig. 12a shows a cluster of the noble $AlTa_3$ precipitates hanging on the edge of a pit in the Al-Ta alloy. Pitting most likely initiates in the Al-rich phase where this phase comes in contact with the $AlTa_3$. As the more active aluminum-rich matrix is depleted, the more noble $AlTa_3$ precipitates are eventually undermined and fall to the bottom of the pits as they grow. These micrographs, again, reveal the star-like morphology of the $AlTa_3$ precipitates. The micrographs of the pitted Al-W alloy also show depletion of the Al-rich matrix, which leaves the more noble WAl_{12} precipitates behind.
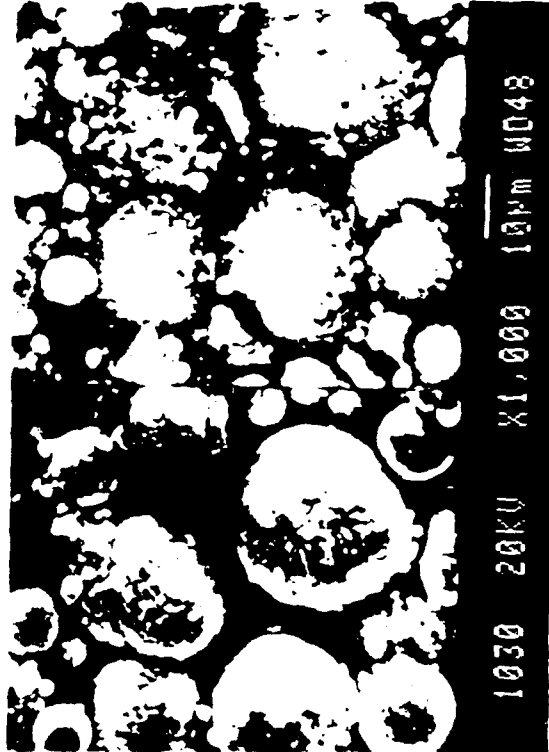
Figure 6. SEM micrographs of AlW (top) and AlTa (bottom) powders. The backscattered electron image (lower left) enhances the contrast between the Al matrix and the Ta rich precipitates.

15
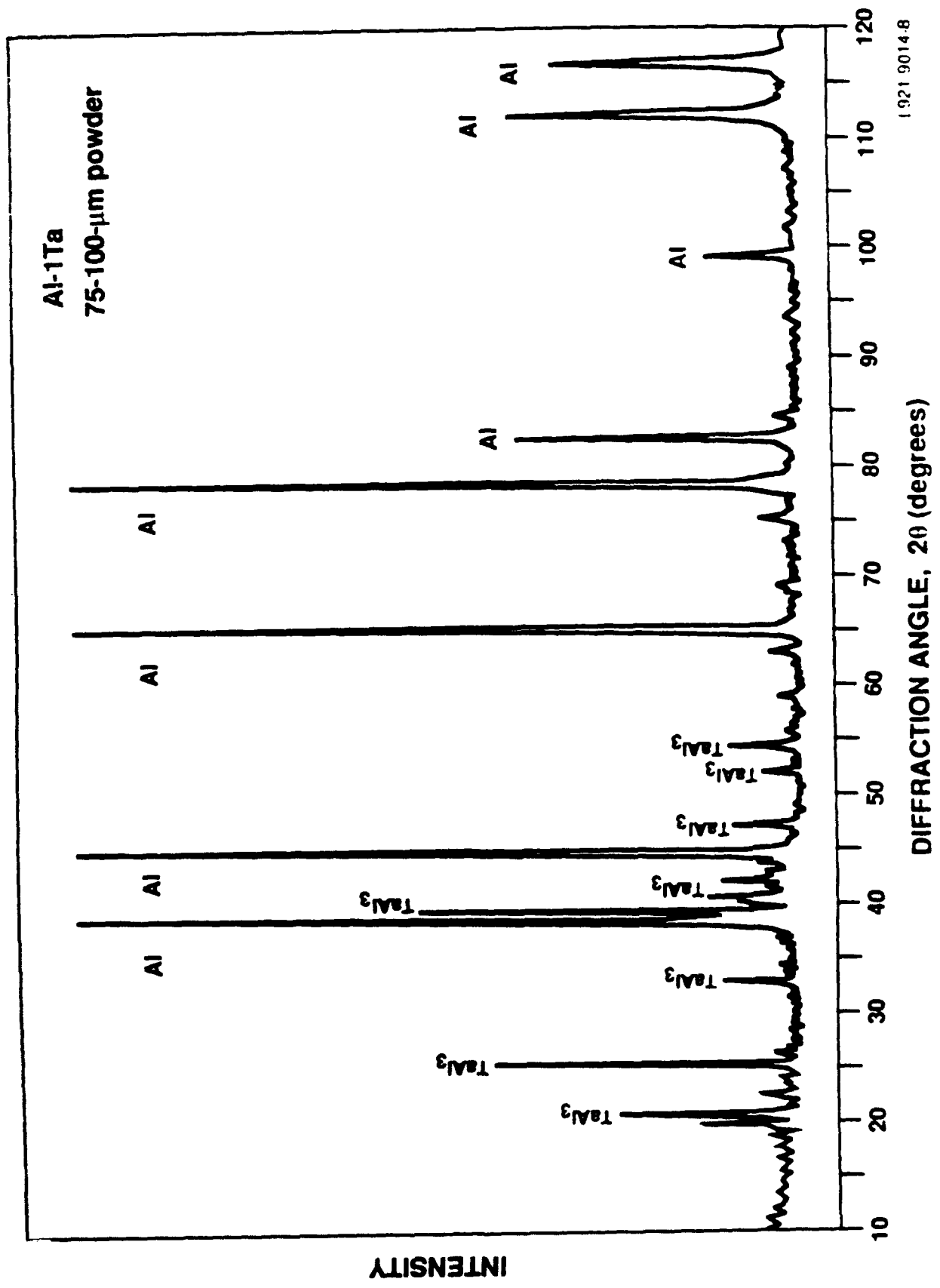
Figure 7   X-ray diffraction spectrum for RS Al-1% Ta powder (10- to 30-μm particle size)

16
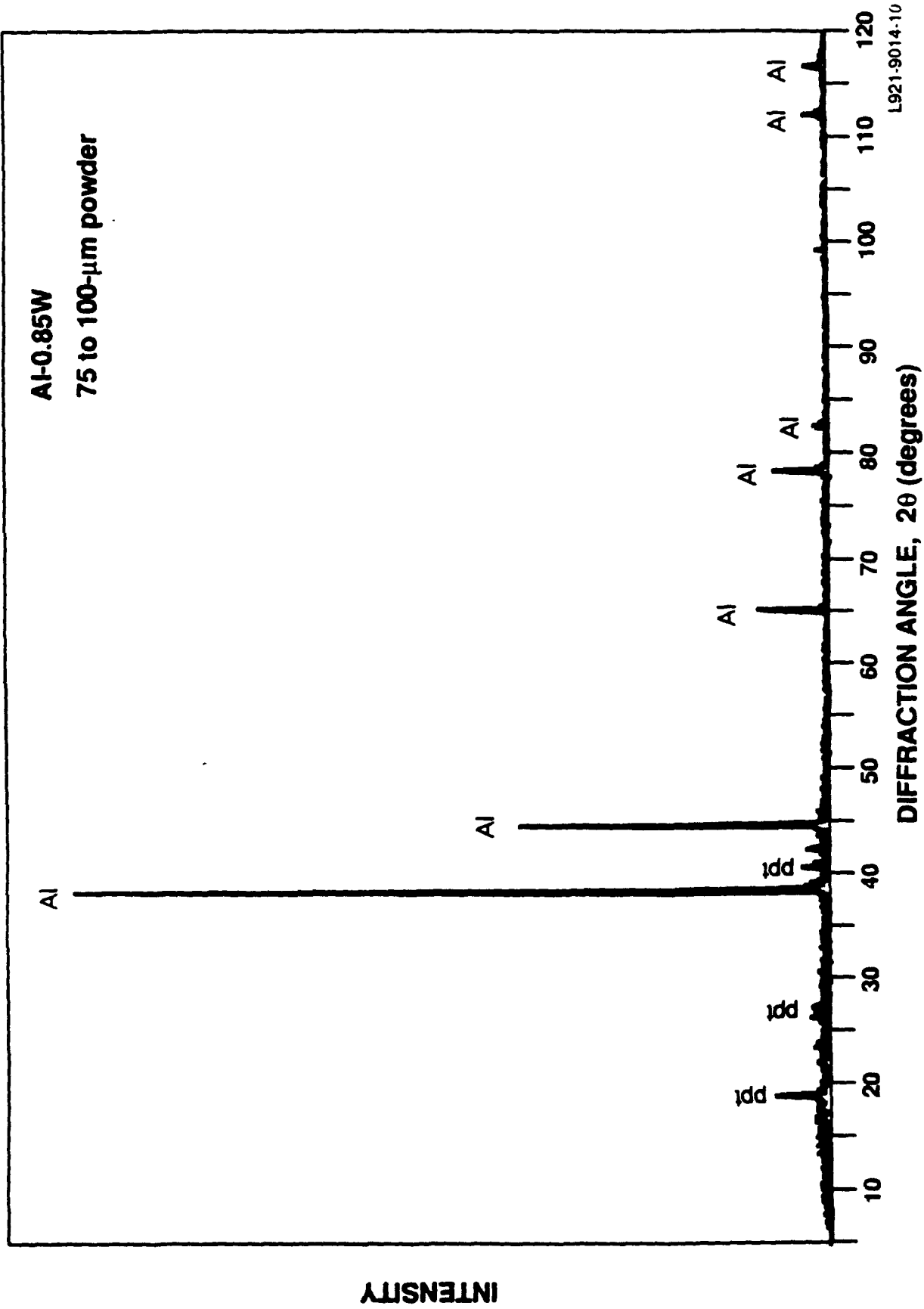
Figure 8   X-ray diffraction spectrum for RS Al-0.85%W powder (75- to 150-μm parti-
cle size).

17
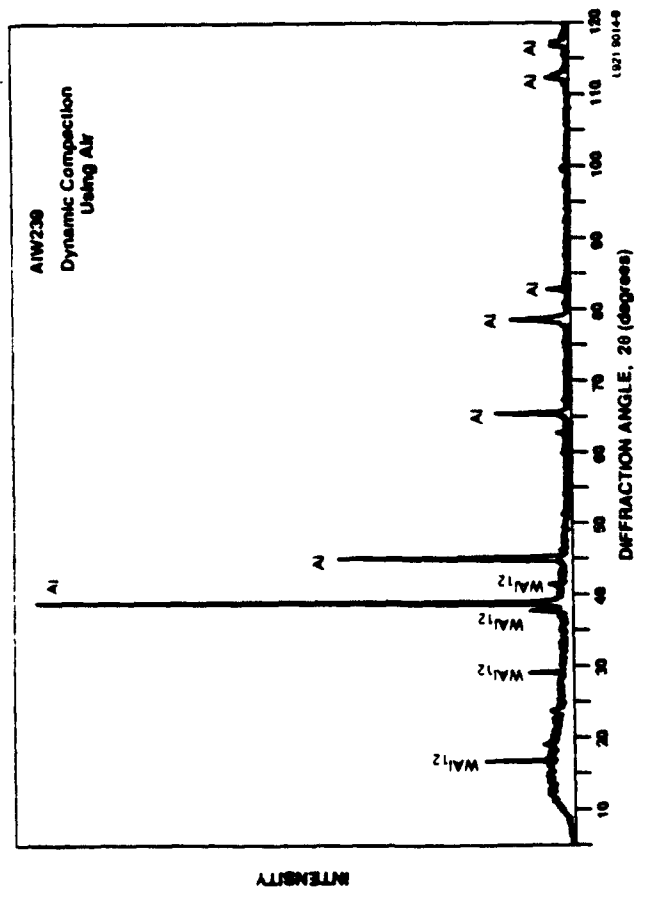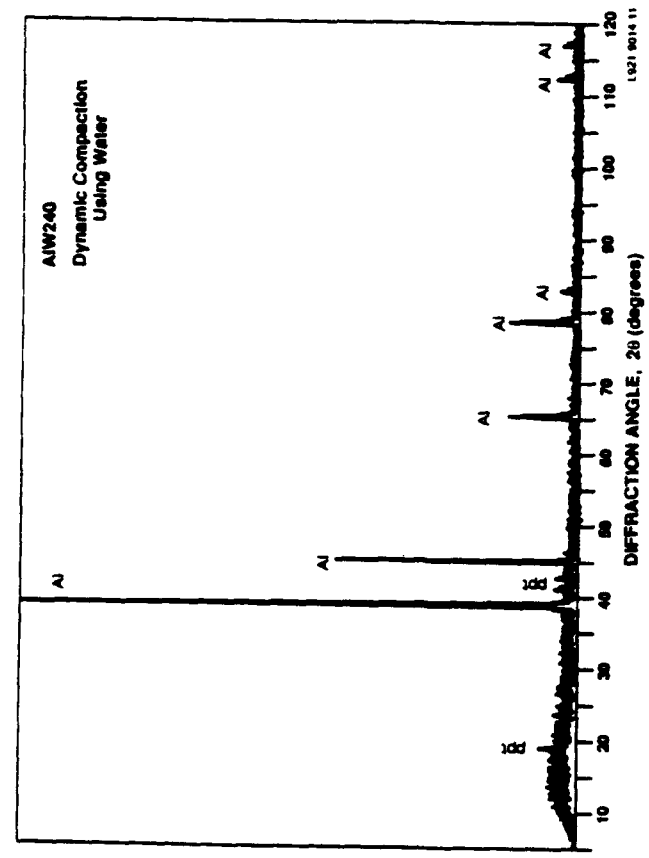
Figure 9   X-ray diffraction spectra for the RS Al-0.85%W powder (75- to 150-µm
            particle size) after dynamic compaction using a) the air technique and b)
            using the water technique.

18
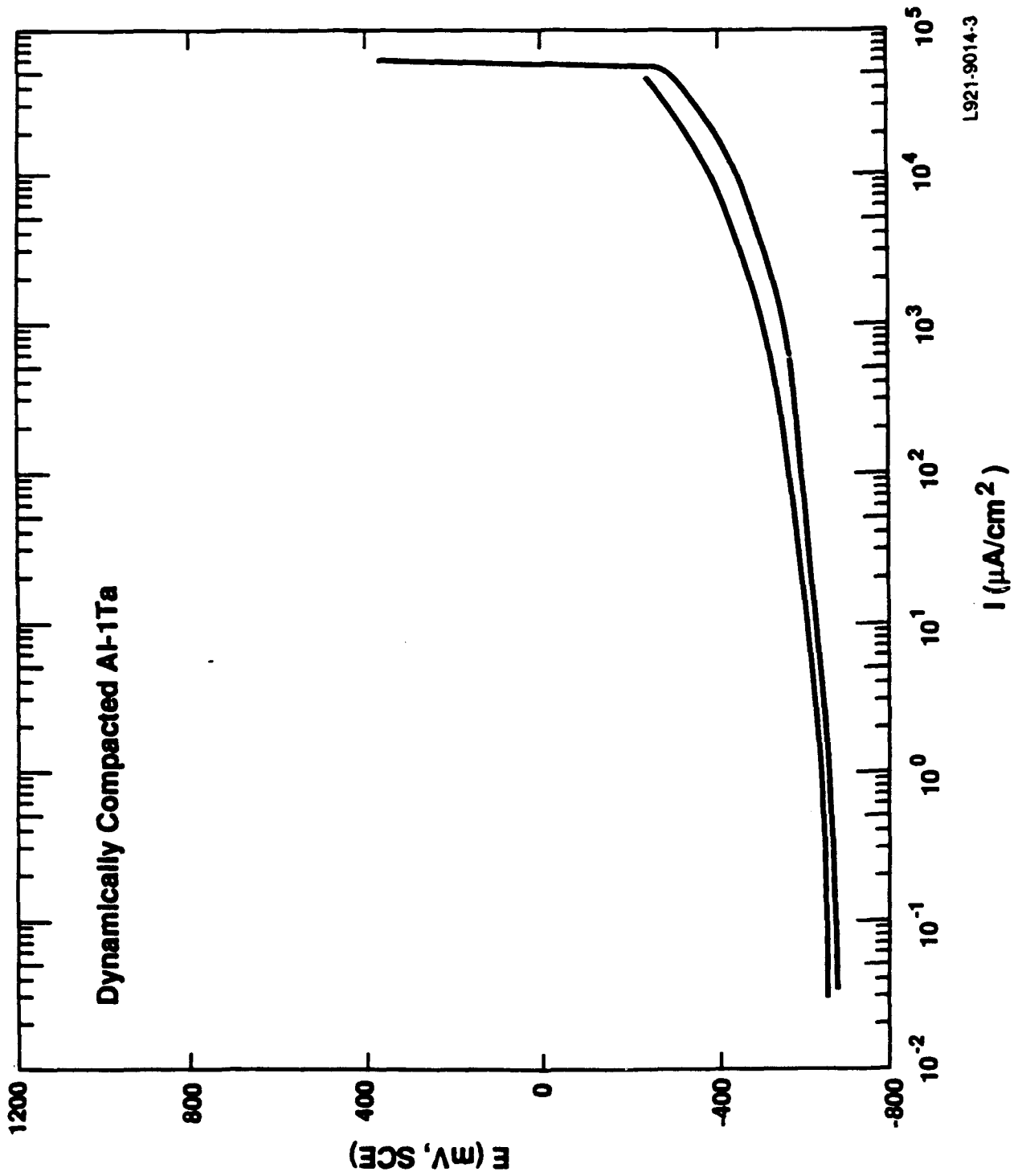
Figure 10 Anodic polarization behavior for the dynamically compacted Al-1Ta alloys in 0.1M KCl.

L921-9014-3

19
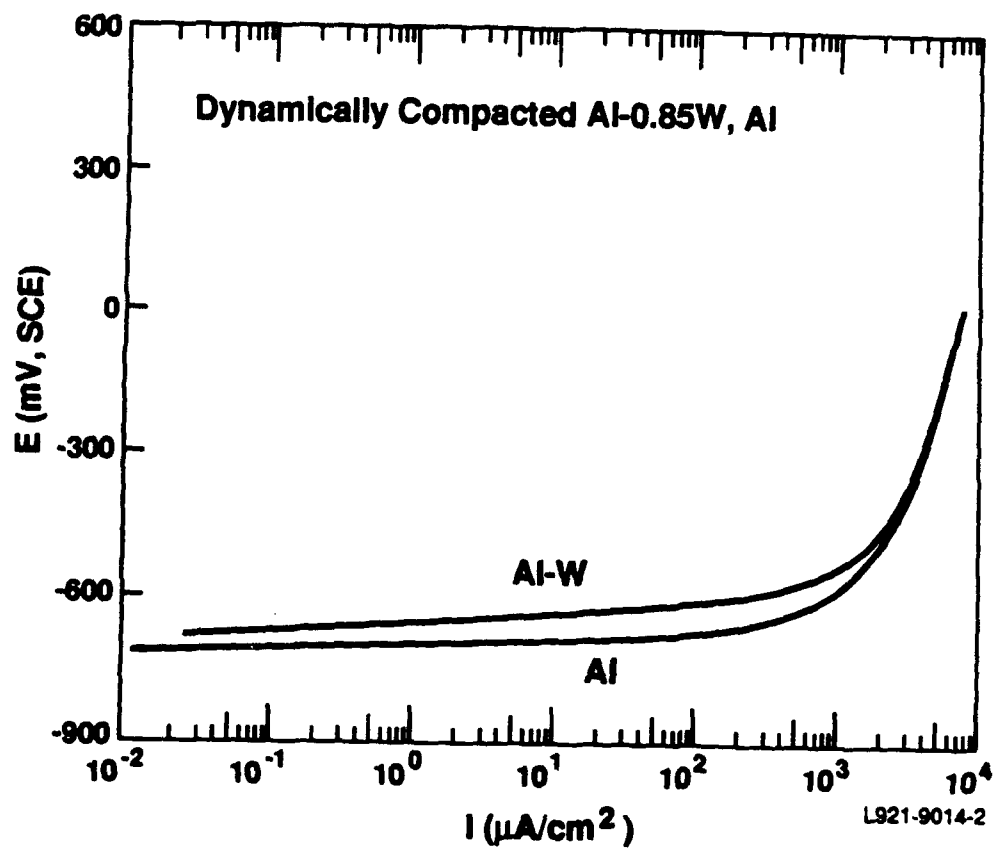
Figure 11   Anodic polarization behavior for the dynamically compacted Al-0.85W alloy and pure Al in 0.1M KCl.

20
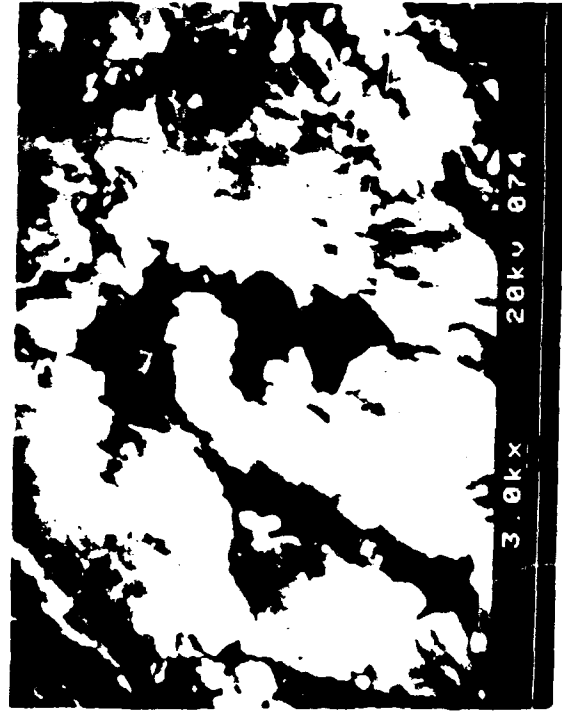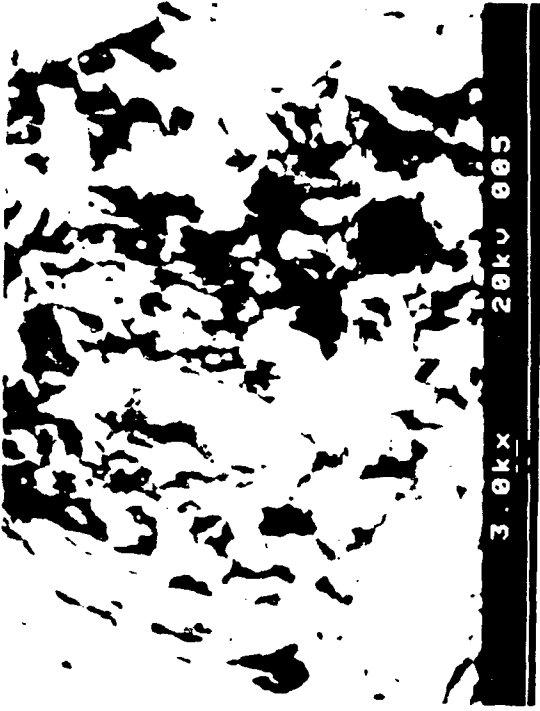
Figure 12. SEM micrographs of pits in AlW (top) and AlTa (bottom) specimens.

21

Although the dynamically consolidated alloys exhibited poor corrosion perfor-
mance, the consolidation process itself was believed to be successful. For the Al-Ta
alloys and the Al-W alloys compacted in water, the precipitates detected in the bulk
specimens were the same as those found in the powders prior to consolidation, and
SEM micrographs revealed that the precipitates in the consolidated material were
similar in size to those in the original powder. Thus, the consolidation process does
not appear to have contributed to the formation of new precipitates or to substantial
growth of the existing ones. Poor corrosion performance of the dynamically consoli-
dated alloys was due to the presence of a second phase, which set up microgalvanic
cells and led to pitting. If RS powders could be produced without precipitates it is likely
that a corrosion-resistant alloy could be formed using a dynamic consolidation pro-
cess.

Thin-Film Alloys

AlAu alloys

The Al-Au system, a material whose solute should not oxidize and form part of the
passive film, but whose presence might lead to the same structural changes in the
passive film that we observed for the Al-Mo alloys and that may also be responsible for
enhanced passivity in the Al-W alloys was chosen as control. The Al-14Au and Al-
11Au alloys that were produced by sputter deposition were polycrystalline with grain
sizes on the order of 0.1 μm. Precipitates identified as Al_2Au were found in the Al-
14Au alloy and may have contributed to preferential dissolution of the Al matrix for
these alloys. Both alloys experienced significant corrosion upon exposure to 0.1M KCl,
i.e., no evidence of passivity. Spontaneous corrosion was further indicated by surface
analysis of the specimens held at E_{oc}, which showed a relatively thick oxidized layer
(Fig. 13) with some variation in thickness (3 to 20 nm). After polarization, the speci-
mens exhibited a dealloyed appearance. Preferential dissolution of the more active Al
in these alloys is believed responsible for their poor corrosion performance. The Al_2Au
precipitates may have also contributed to preferential dissolution of the Al matrix. Sur-
face analysis of the alloys revealed that the oxidized film was entirely aluminum ox-
ide/hydroxide; no Au was detected. Thus, while we were successful in producing an
alloy with no oxidized solute in the passive film, the large potential differences
between the Al and the Au, combined with the significant concentration of Au in the
alloys, appears to have resulted in dealloying instead of the intended result.

22

Al-Au
E_{OC}, 0.1M KCl

Au 4f

98.9   76.7

Al 2p

79.9   57.7

BINDING ENERGY (eV)
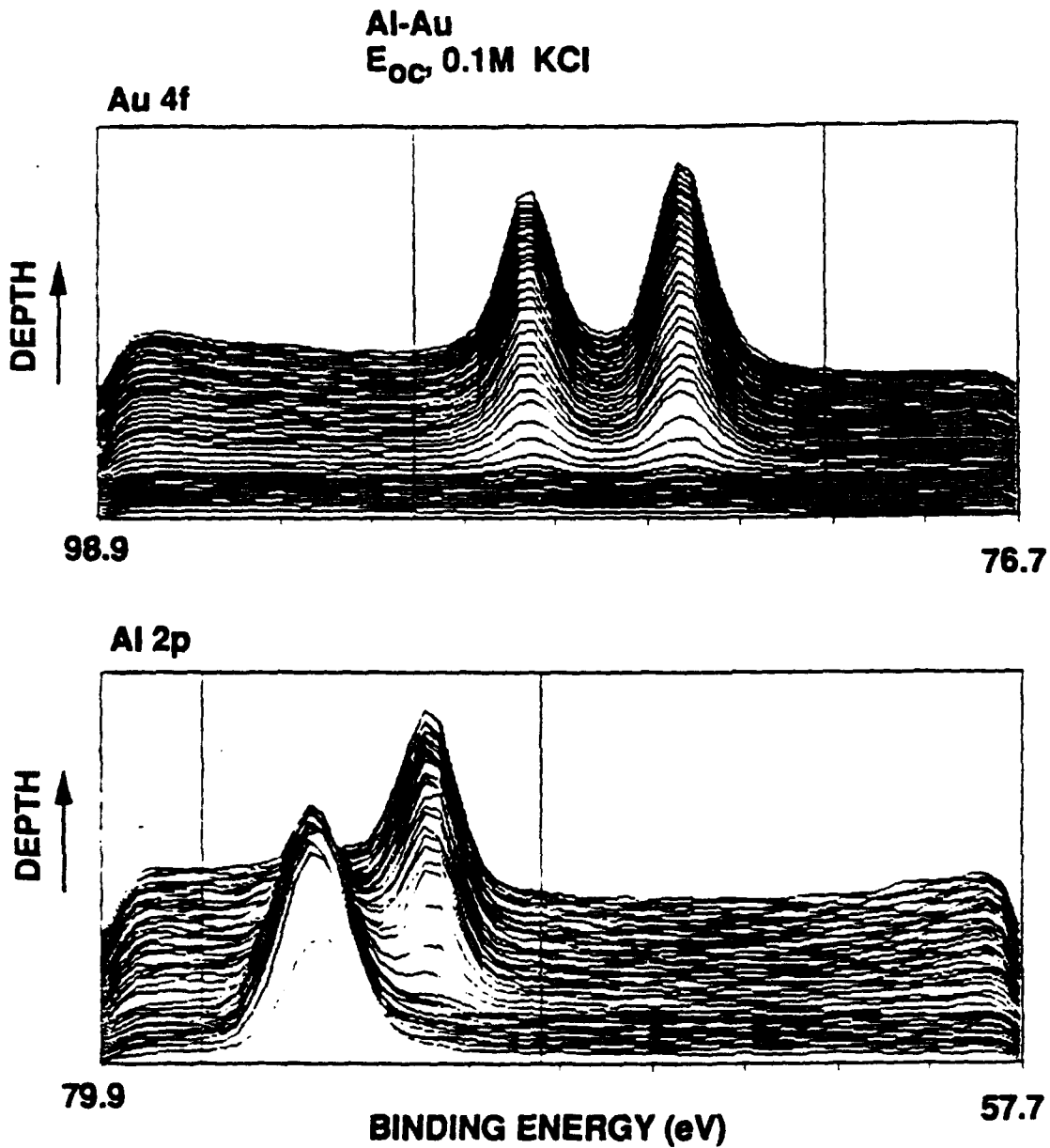
L921-9007-10

Figure 13. Au 4f and Al 2p photoelectron spectra as a function of sputter time (and, hence, depth).

23

Microstructure

The Al-W specimens (~3-7%) examined by TEM and XRD this year were all crystalline with grain sizes ranging from 0.3-1.0 μm (Fig. 14). Unlike last year, no amorphous specimens were observed. Previously, we had proposed that the amorphous material was a function of solute concentration and localized cooling rate.[7] Our current results support this hypothesis and suggest that small changes in our sample holder and in how the wafer is mounted affected the local thermal conductivity between the holder and the wafer and, hence, the localized substrate temperature. At higher solute concentrations, amorphous material is formed at lower cooling rates or higher substrate temperature. Thus, Frankel[9] and Shaw and Moshier[42] observe amorphosity with their high concentration alloys.

The grain size of the specimens reported here is larger than those reported earlier,[29] but the breakdown potentials are comparable (Fig. 15). This conflicts with the observations reported by Inturi and Szklarska-Smialowska[21] who saw a correlation between grain size and E_p. Our results (Fig. 15) show a possible relationship at small grain size, although with a different slope than the results of Inturi and Szklarska-Smialowska. However, the results at larger grain size do not correlate at all, suggesting that passivity mechanisms involving grain boundaries cannot explain the corrosion resistance of these alloys in general. This and other proposed mechanisms will be discussed below.

Behavior at high and low pH values

The anodic polarization behavior for an Al-3.6W alloy was evaluated in chloride solutions of varying concentrations and pH values ranging from 0 to 9.6. The experiments conducted and the characteristic parameters taken from the polarization data are summarized in Table 3 and Figs. 16-20. Figure 18 reveals that passivity is observed for the Al-W alloys as the pH is decreased. The passive range is smaller at the lower pH values and the passive current density increases with decreasing pH. A comparison of the polarization behavior of the Al-W alloys with pure W at pH 3 (Fig. 18) reveals similar passive current densities for the low pH curves, suggesting that the alloy passive film at low pH contains significant amounts of oxidized W. Surface analysis of these alloys, discussed below, confirms this. Comparable pitting potentials
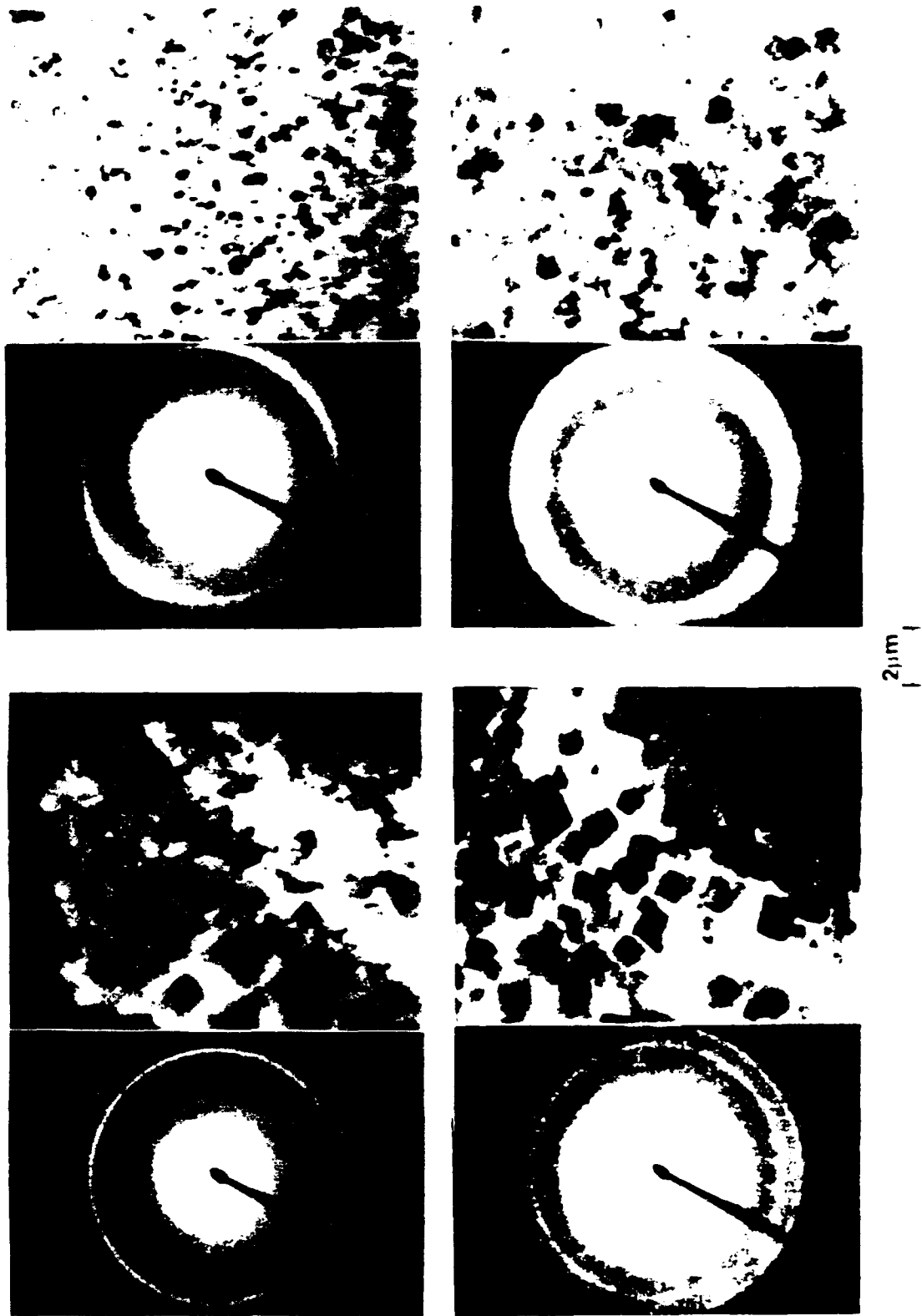
Figure 14   TEM and selected area diffraction images of AlW alloys, clockwise from lower left Al3W, Al 3W, Al 5W, and 5W

2μm
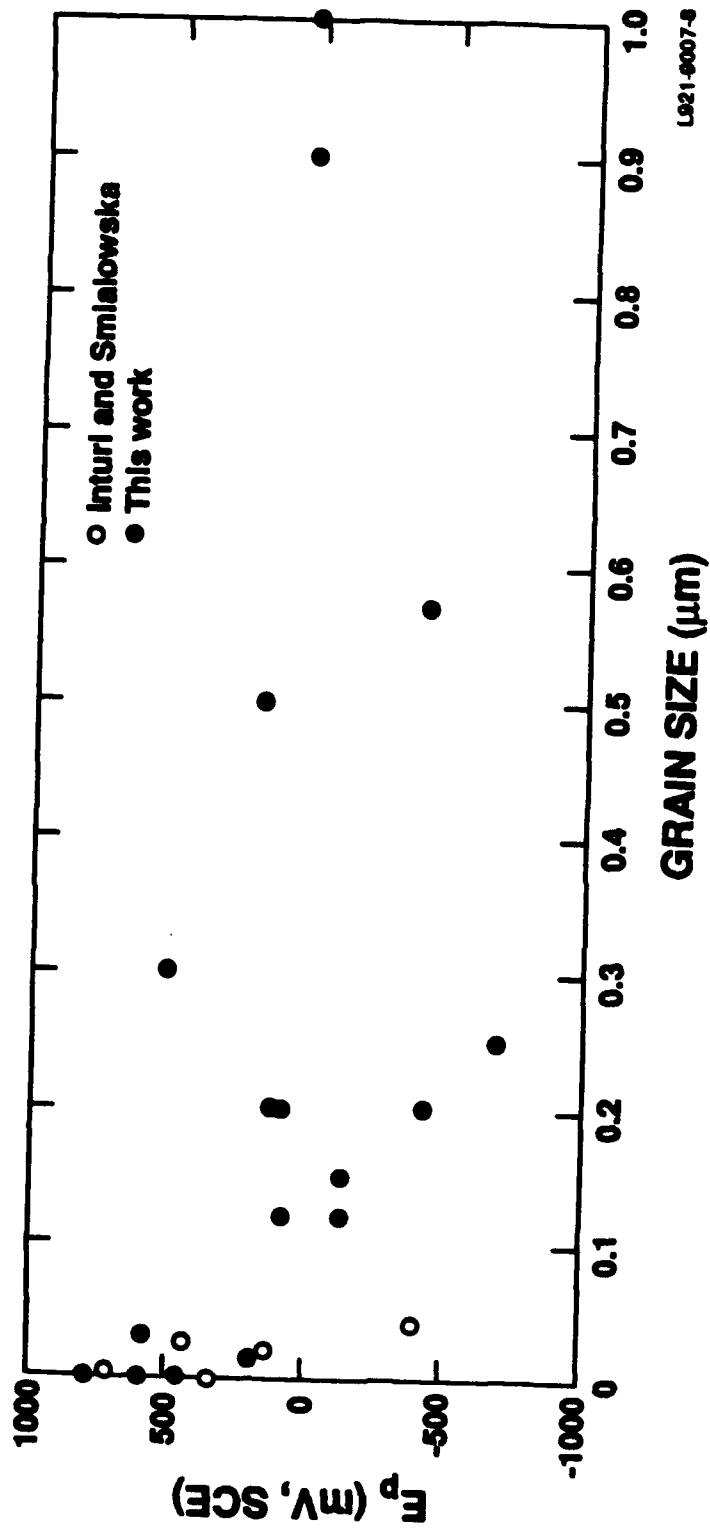
Figure 15. Pitting potential as a function of grain size for a variety of nonequilibrium Al alloys. The data are from References 1-5, 21, and 22.

26
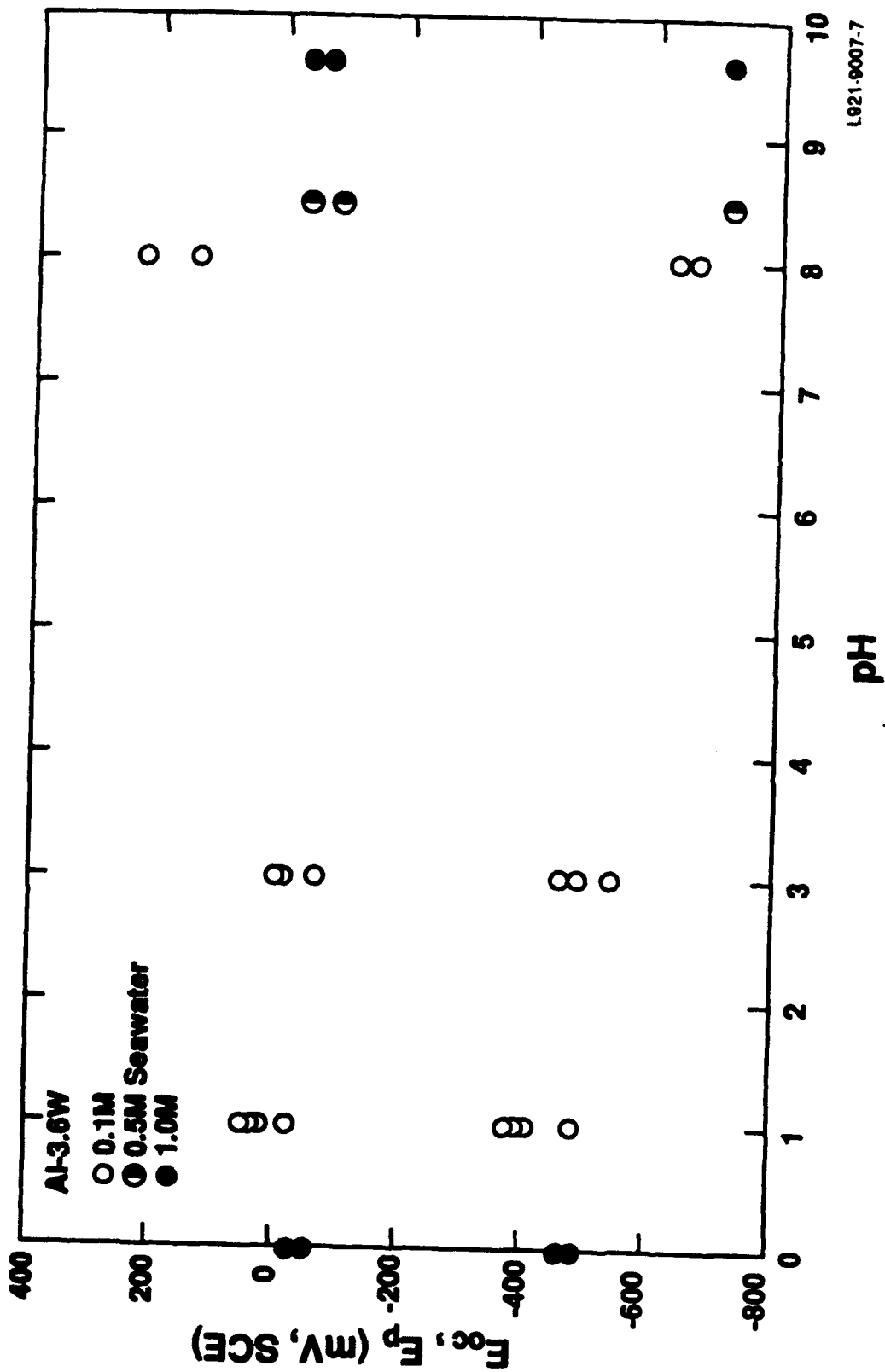
Figure 16. Open circuit and pitting potentials for the Al-3.6W specimens reported in Table 3.

L921-9007-7

27
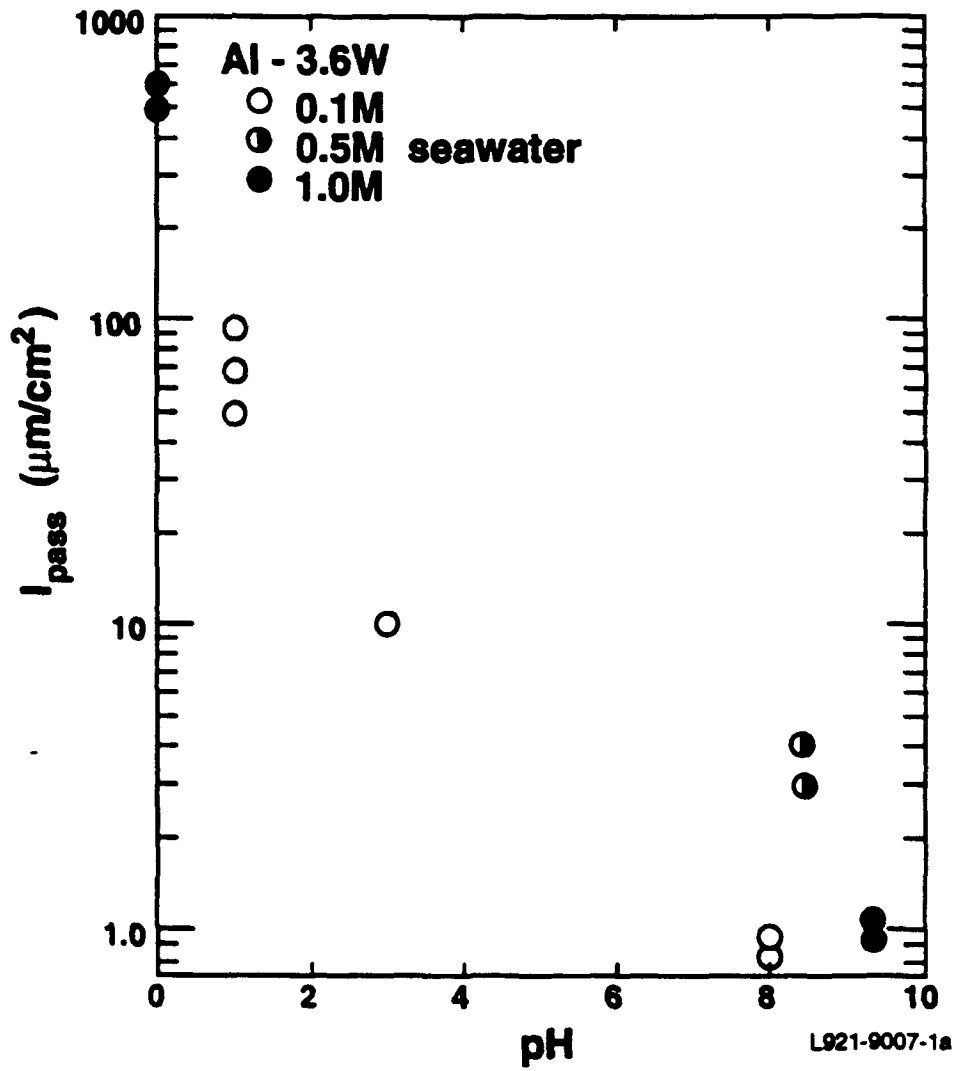
Figure 17. Passive current density of the Al-3.6W specimens reported in Table 3.
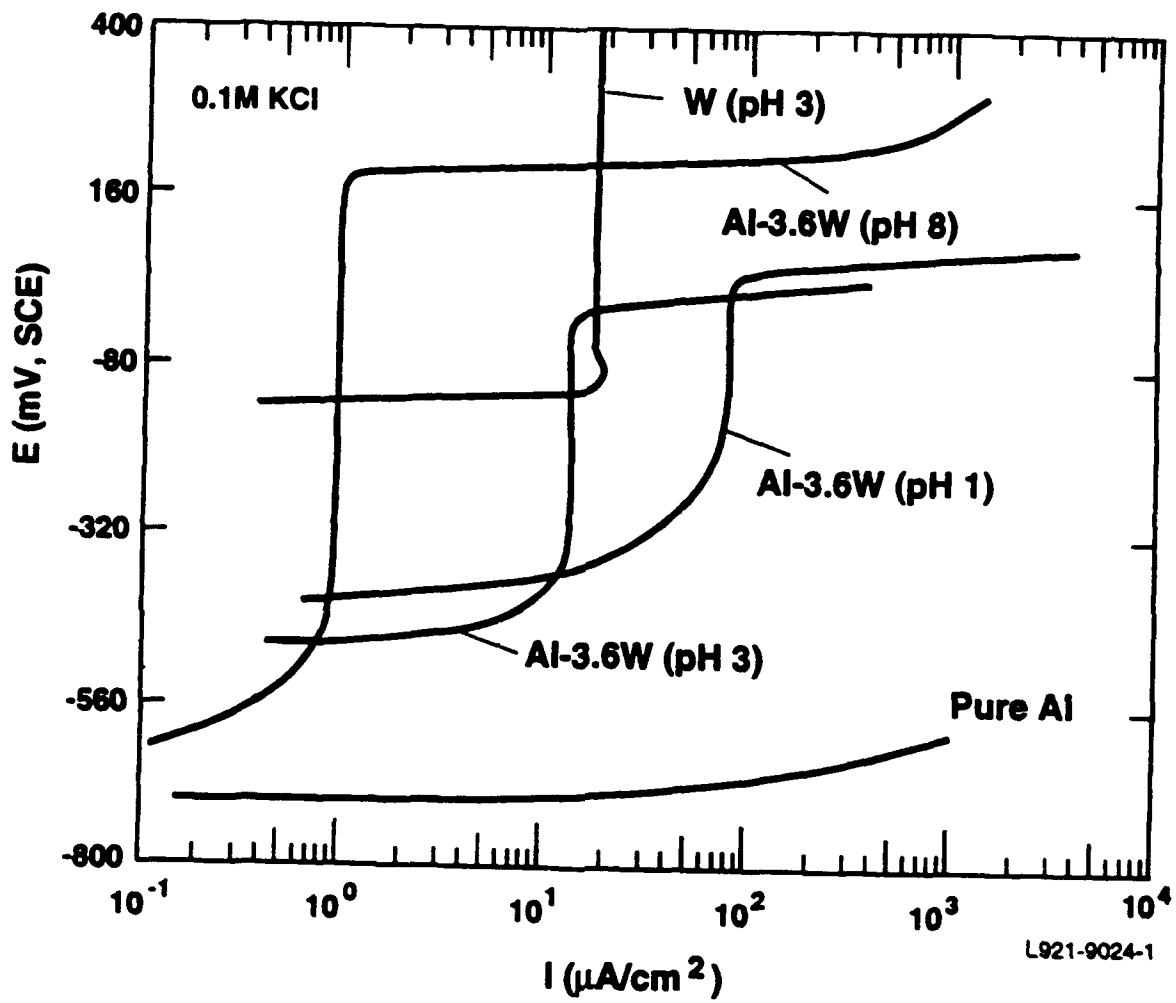
Figure 18   Anodic polarization behavior of thin film Al-3.6W alloy as a function of pH
compared to pure W and pure Al in 0.1M Cl⁻ (averaged data)
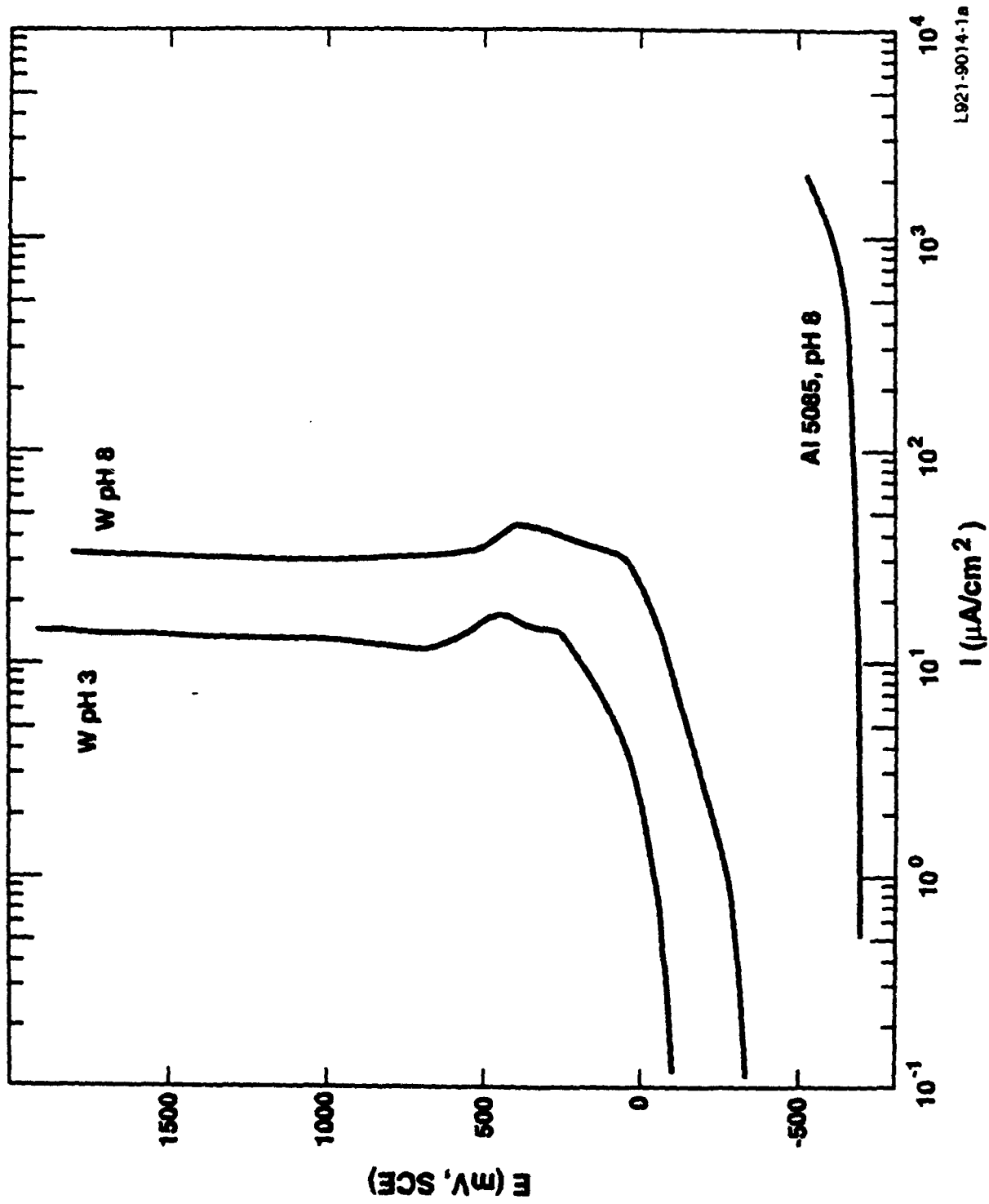
Figure 19   Anodic polarization behavior of pure W at pH 8 and 3 and 5086 Al at pH 8 (total [Cl⁻] = 0.1M).

L921-9014-1a

30
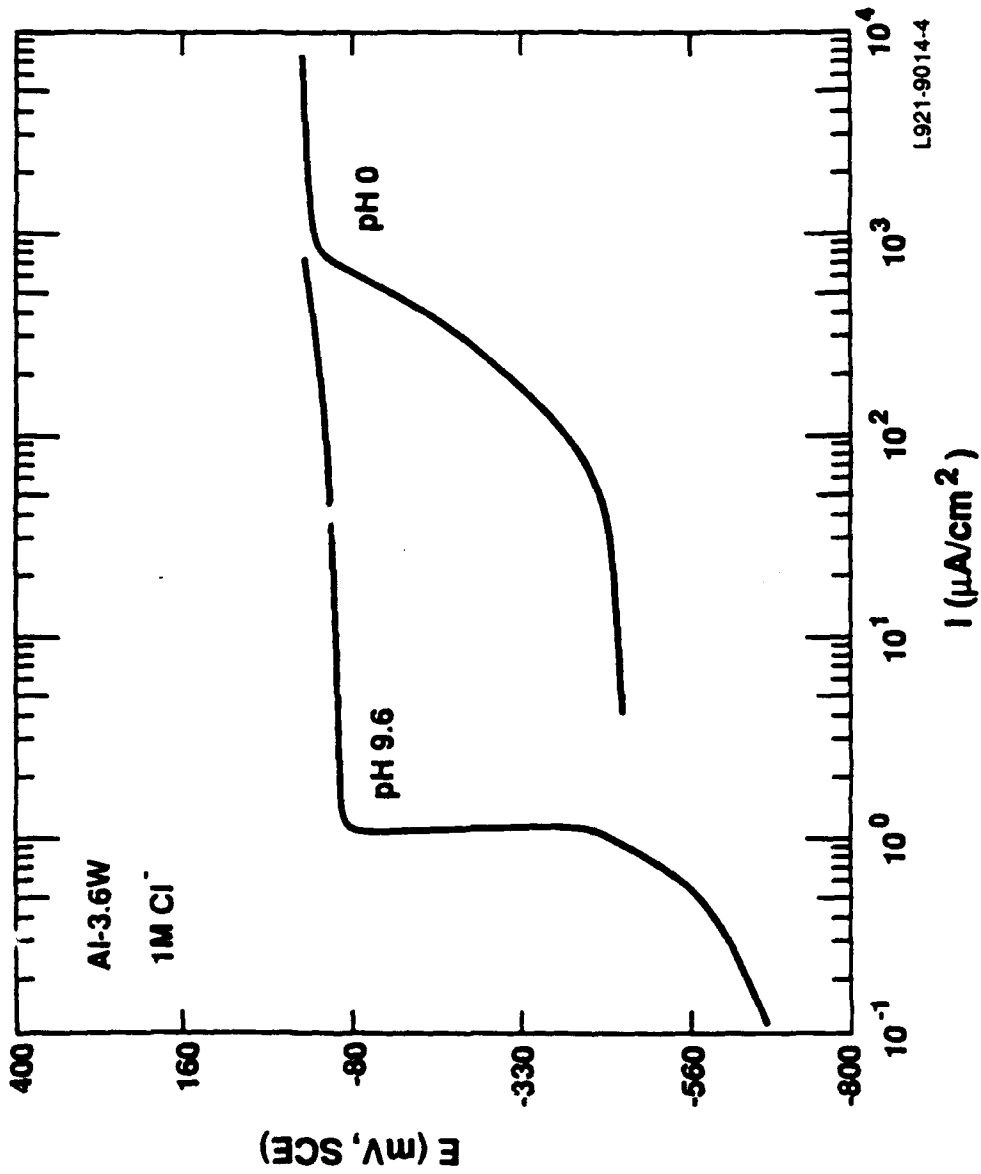
Figure 20   Anodic polarization behavior of thin-film Al-3.6 W alloy in 0.1 M KCl (pH 9.6) and 1.0 M HCl (pH 0) (averaged data).

Table 3. Anodic Polarization Behavior

|	[Cl⁻]	pH	E_p(mV, SCE)	i_p ($\mu A/cm^2$)	E_{oc} (mV, SCE)	Solution
Al-14W*	0.1M	8	513	1	-542	KCl
Al-14W*	0.1M	8	478	1	-582	KCl
Al-10W*	0.1M	8	451	0.6	-710	KCl
Al-10W*	0.1M	8	376	0.8	-686	KCl
Al-3.6W	0.1M	8	144	0.8	-632	KCl
Al-3.6W	0.1M	8	228	0.9	-661	KCl
Al-3.6W	0.1M	3	0	10	-454	HCl/KCl
Al-3.6W	0.1M	3	-7	10	-455	HCl/KCl
Al-3.6W	0.1M	3	0	10	-480	HCl/KCl
Al-3.6W	0.1M	3	-61	10	-536	HCl/KCl⁺
Al-3.6W	0.1M	1	20	50	-478	HCl
Al-3.6W	0.1M	1	42	95	-381	HCl
Al-3.6W	0.1M	1	32	70	-374	HCl
Al-3.6W	0.1M	1	-15	70	-402	HCl⁺
Al-3.6W	0.5M	8.4	-35	4	-714	Seawater
Al-3.6W	0.5M	8.4	-84	3	-717	Seawater
Al-3.6W	1.0M	9.6	-31	0.95	-714	KCl
Al-3.6W	1.0M	9.6	-66	1	-715	KCl
Al-3.6W	1.0M	0	-15	600	-461	HCl
Al-3.6W	1.0M	0	-46	500	-478	HCl
Pure Al	0.1M	3	-710	22 **	-917	KCl
Pure Al	0.1M	3	-701	—	-701	KCl
Pure Al	0.1M	1	-695	50 **	-916	KCl
Pure Al	0.1M	1	-700	20 **	-906	HCl
Pure Al	1.0M	0	-775	100 **	-916	HCl
Pure Al	1.0M	0	-773	251 **	-854	HCl
Pure W	0.1	8	none	32	-311	KCl
Pure W	0.1	3	none	14	-128	HCl

* Approximate concentration
** Average
+ Scan rate = 0.02 mV/s

(despite the differences in chloride concentration) were noted at pH 1 and 3, with the values at the lower pH being slightly more noble. The reason for the slightly higher pitting potential at pH 1 is not known, but it could be related to higher oxidized W concentrations in the passive film. Fig. 19 shows that no pitting potential is observed for the pure W at potentials less than 2000 mV and that as the pH is reduced, the i_p for W decreases. This implies that the W passive film that forms at low pH is more protective, or stable, than the film that forms at pH 8. Also included in this figure is the polarization behavior for 5086 Al, a corrosion-resistant conventional alloy, at pH 8. Like pure Al, passivity for this alloy is not observed in a 0.1 M chloride solution at potentials greater than 700 mV. Passivity is still observed for the Al-W alloys at a pH of 0, but i_p is now found to vary with potential, exhibiting an average value of approximately 500 $\mu A/cm^2$ as shown in Fig. 20. Also shown in this figure is the polarization behavior for the Al-W alloy in 1.0 M Cl⁻ (pH=9.6). At a pH of 9.6 the Al-W alloy exhibits the same low i_p noted at pH 8, but a lower value for E_p.

The polarization behavior of Al-Ta alloys has been investigated at pH values ranging from 3 to 12. The results are presented in Figs. 21 through 23. In Fig. 21, the anodic polarization behavior for Al-(4-7)Ta can be compared with pure Ta and 5086 Al. The pure Ta is passive over the entire potential range evaluated and appears to undergo some transpassive dissolution at approximately 1400 mV. The passive current density of 0.7 $\mu A/cm^2$ for the Al-Ta alloy is similar to that observed for pure Ta. The most dramatic performance for the Al-Ta alloys was noted at pH 12. Figure 22 reveals a large passive region, extending over 1.5 V, and low passive current densities for an Al-6.75Ta alloy in 0.1 M Cl⁻ with the pH adjusted to 12 (with NaOH). The reason for the increase in current at low potentials is under investigation. Some passivity, although diminished in comparison to the previous results, is also observed at low pH values as illustrated in Fig. 23. The scatter in the data is believed to be related to differences in solute concentration from specimen to specimen. These concentration differences were not present in the Al-6.75Ta alloy tested at a pH of 12 because this alloy was produced using a rotating stage for the substrate.

XPS measurements of Al-3.6W alloys in pH 3 solutions show considerably more W in the passive film (Fig. 24). Whereas the passive film at E_{oc} in neutral solutions had very little oxidized W (0.1-0.2% of the oxidized Al),[7] the amounts of W in the acidic solution were comparable to those of Al (50-60% of the Al) -- an increase of more than 100. Both W^{+4} and W^{+6} are present, in a ratio of 3:2 $W^{+4}:W^{+6}$. Additionally, the oxi-
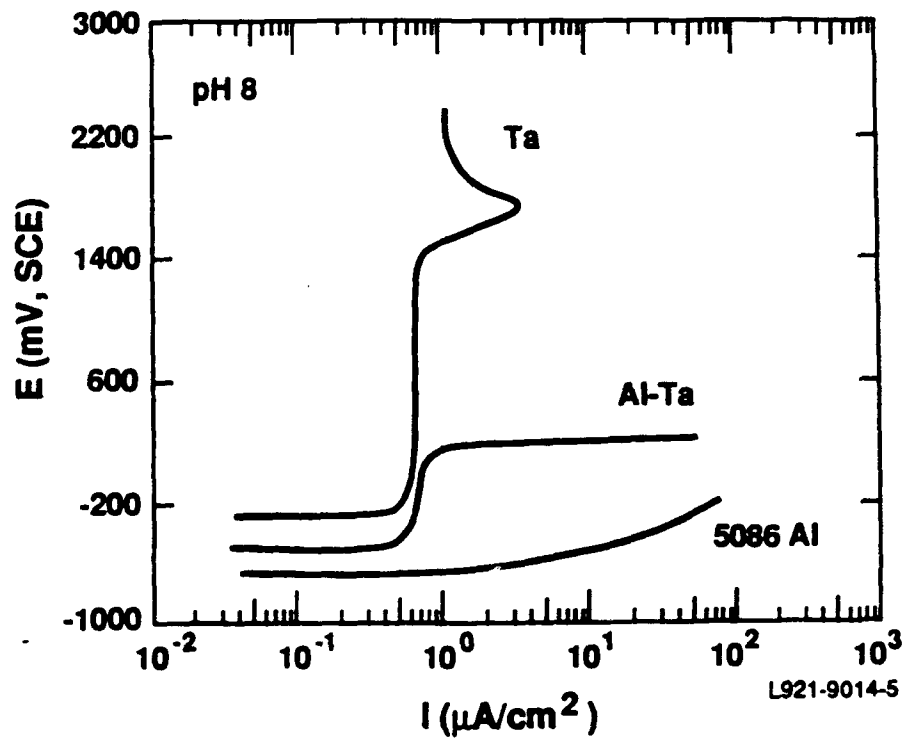
Figure 21   Anodic polarization behavior of an Al-(4 to 7)Ta alloy compared with pure
Ta and 5086 aluminum. (averaged data) in 0.1M KCl.
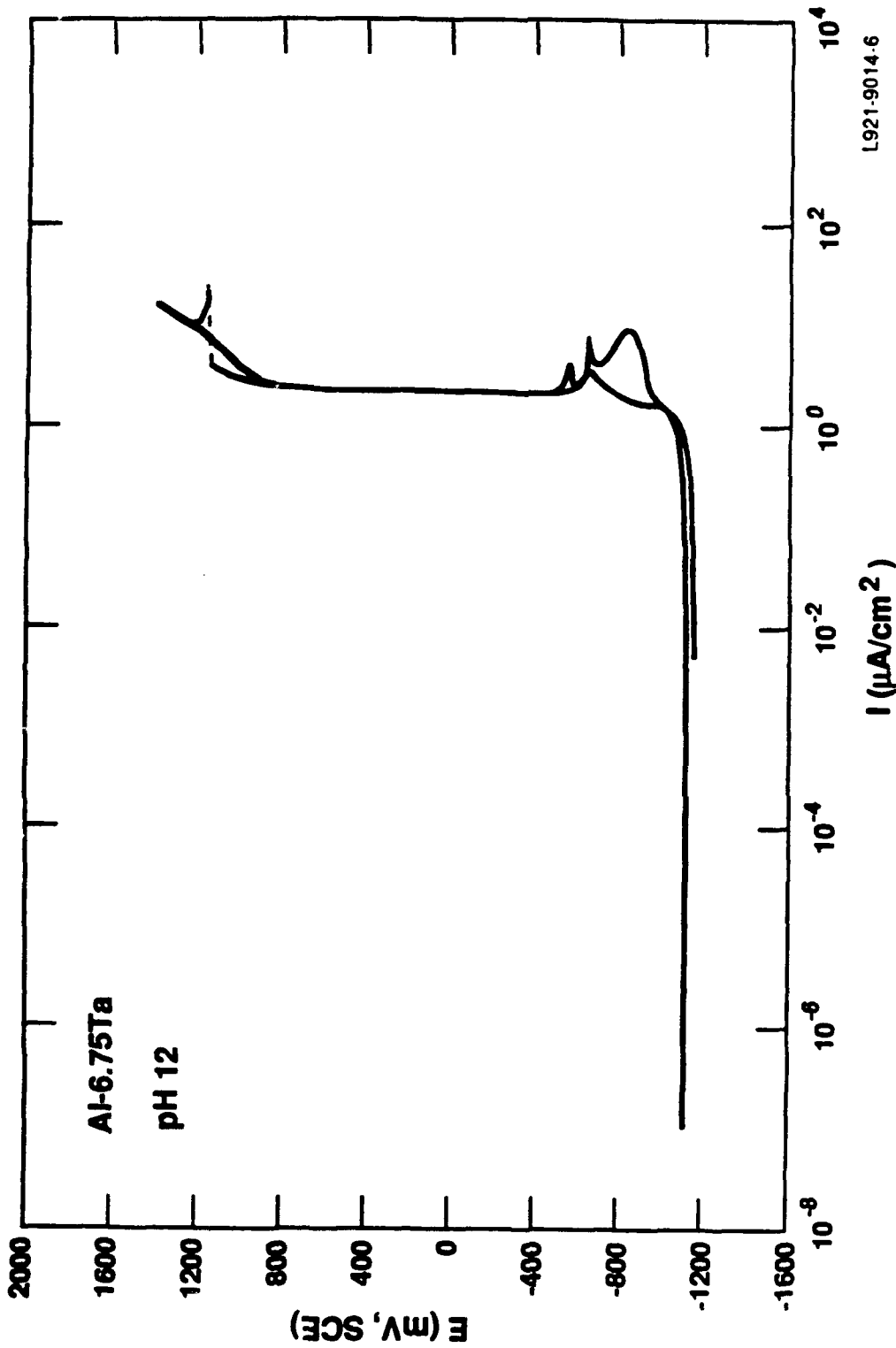
Figure 22   Anodic polarization behavior of an Al-6.75Ta alloy in a 0.1 M Cl- at a pH of
12 (pH adjusted through the addition of NaOH).

L921-9014.6

35
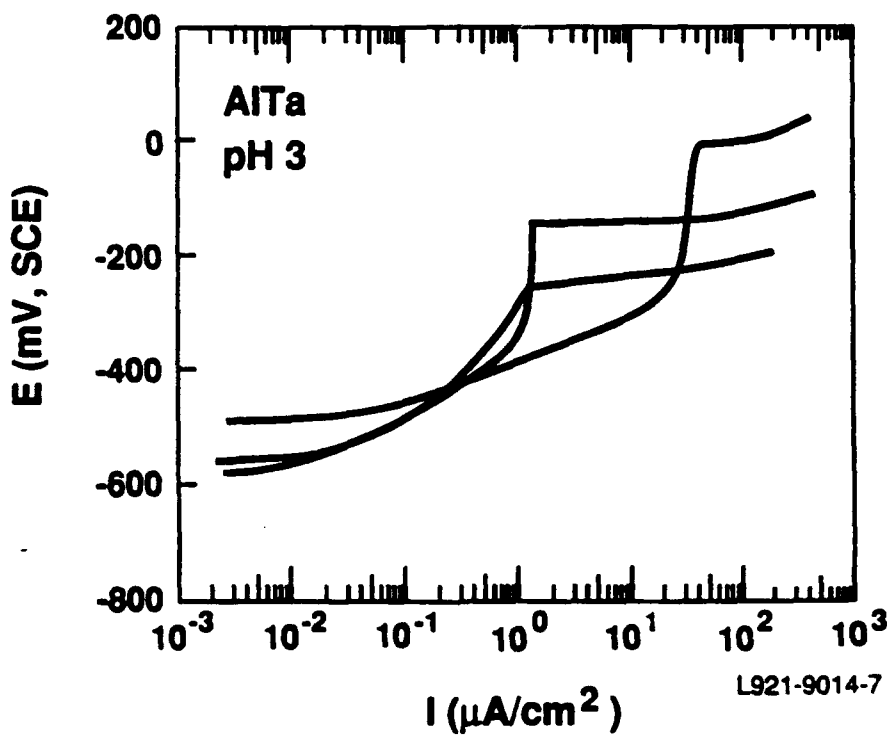
Figure 23. Anodic polarization behavior of replicate specimens of an Al-(4 to 7)Ta alloy at a pH of 3 (total [Cl⁻] = 0.1M).

36
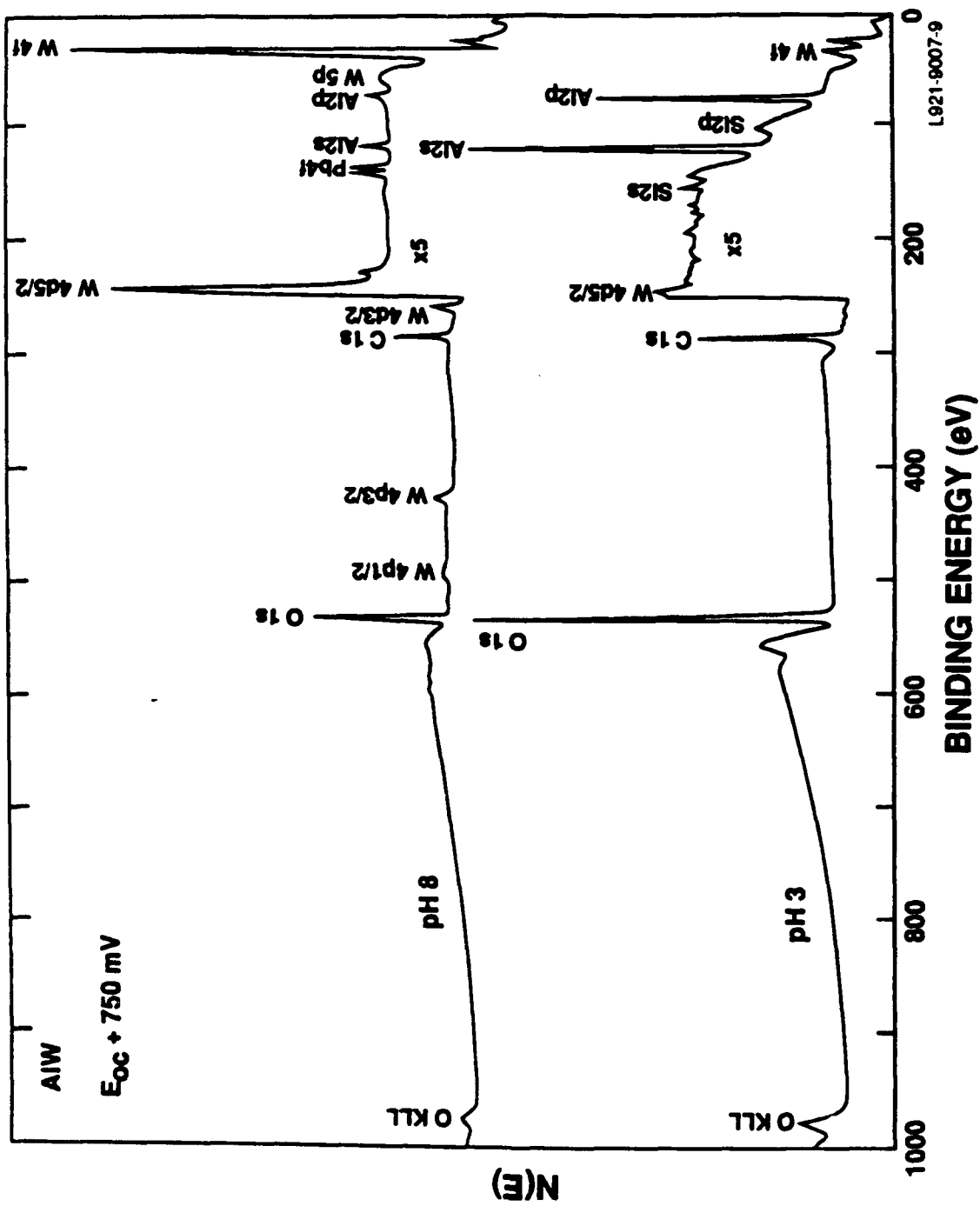
Figure 24. XPS spectra of AlW specimens polarized to an overpotential of ~750 mV in pH 8 and pH 3 0.1 M Cl⁻ solutions.

37

dized aluminum is more hydrated at pH 3; its composition is close to $Al(OH)_3$ whereas films formed at pH 7 were closer to AlOOH.

The passive film at pH 3 is also much thicker than that at pH 7. Although the latter was only 4 nm at E_{oc} and the underlying substrate was clearly observed in the XPS spectra, the signal from the substrate was not detectable following immersion in the acidic solution. The passive film in this case is ~15 nm thick as determined by sputter depth profiling (Fig. 25). There appears to be a gradient in composition with the passive film being relatively W-rich at the surface and more Al-rich near its interface with the substrate.

The chemistry of the passive film changes slowly during polarization up to E_p (Fig. 26). Over the course of the passive region, the ratio of W to Al tends to increase even further with increasing overpotential as shown in Fig. 27.

It is interesting to compare our results to those of Yoshioka et al.[19]. They polarized amorphous Al-15W and Al-45W specimens in deaerated 1 M HCl. Although their electrolyte has a higher Cl⁻ concentration and a lower pH, several trends that we noted in going from pH 8 to pH 3 are also observed in their electrolyte. Little oxidized W is detected prior to immersion into the solution, but upon immersion, the passive film becomes enriched in oxidized W. In both acidic solutions, the fraction of oxidized W increases during polarization with the passive film at pH 3 having approximately equal amounts of W and Al; in 1 M HCl, is entirely oxidized W. Each passive film is thicker than that in near-neutral solutions. Nonetheless, the passive film in 1 M HCl is thin enough for the substrate signal to be detected at E_{oc} and at the first polarization step (50- to 100-mV overpotential). We attribute the thinner film and the lower oxidized Al concentration to increased solubility of Al in the more acidic solution. Although the passive current density is very high in the HCl solution (see also Table 3), Yoshioka et al. report no breakdown during polarization up to 500 mV(SCE). They attribute this passivity to a passive film consisting entirely of WO_3. Our lower concentration alloys did pit in 1 M HCl at ~ -30 mV (SCE) (Table 3), but we have no XPS data to indicate whether the passive film of Al-3.6W alloys would also be WO_3 with no oxidized Al.

At open circuit and at low overpotentials, Yoshioka et al. and we both observe multiple W oxidation states. Initially, they report W^{+4}, W^{+5}, and W^{+6}, with the W^{+4} disappearing after first overpotential and the W^{+5} state developing different chemistry at the
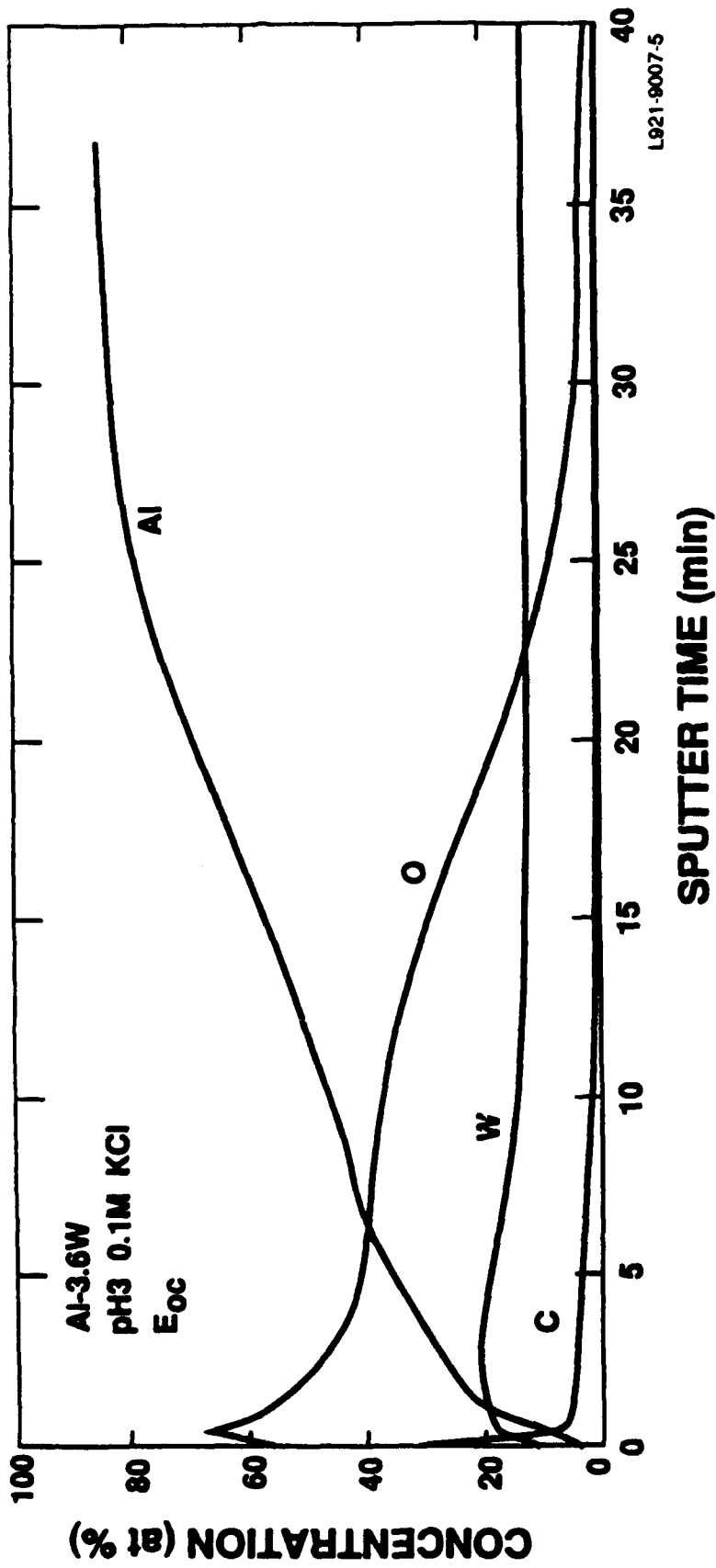
Figure 25. XPS sputter depth profile of an Al-3.6W specimen at E_{oc} in a pH 3 0.1 M Cl⁻ solution.
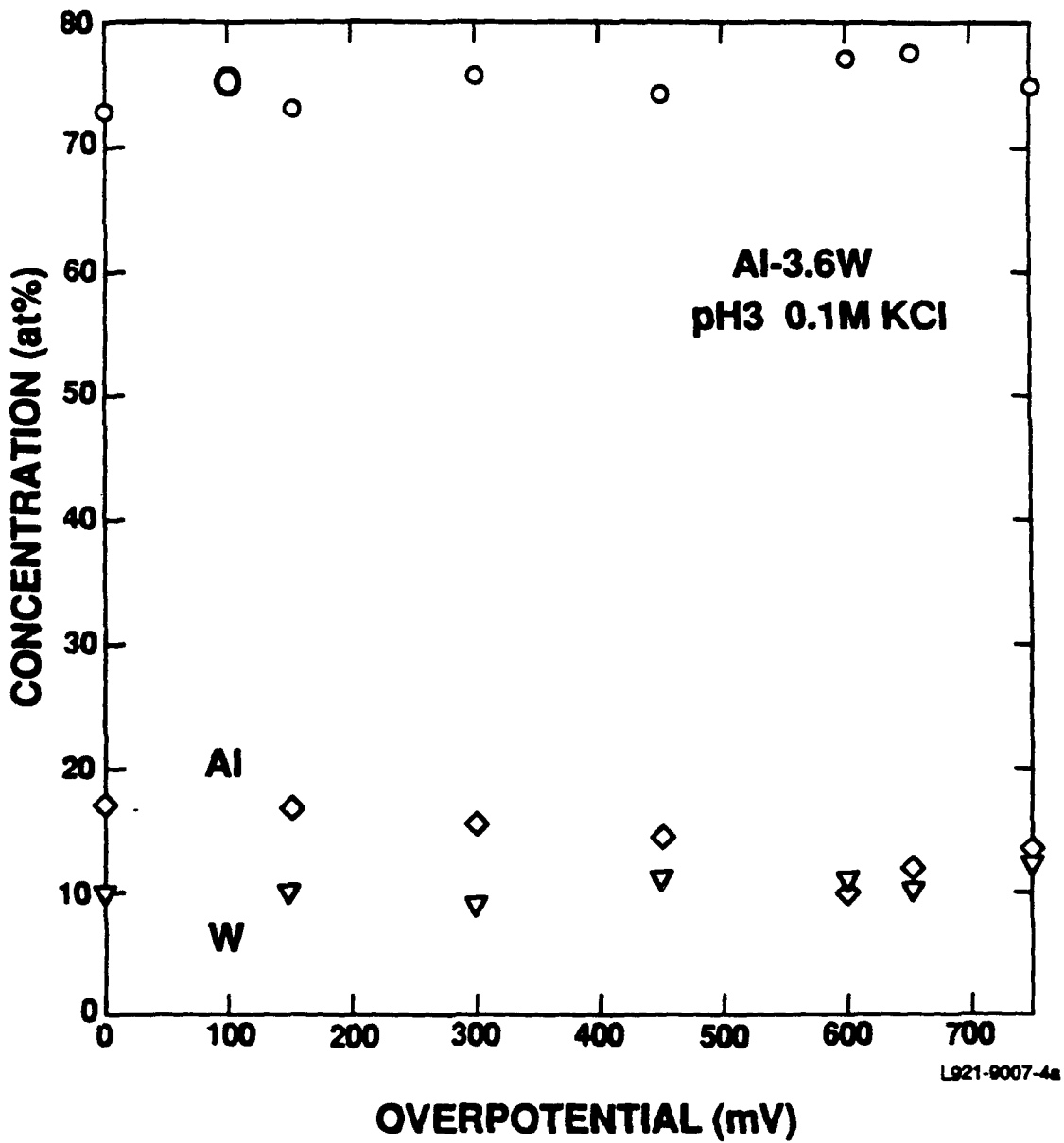
Figure 26. Surface chemistry of an Al-3.6W specimen as a function of overpotential in a pH 3 0.1 M Cl⁻ solution.
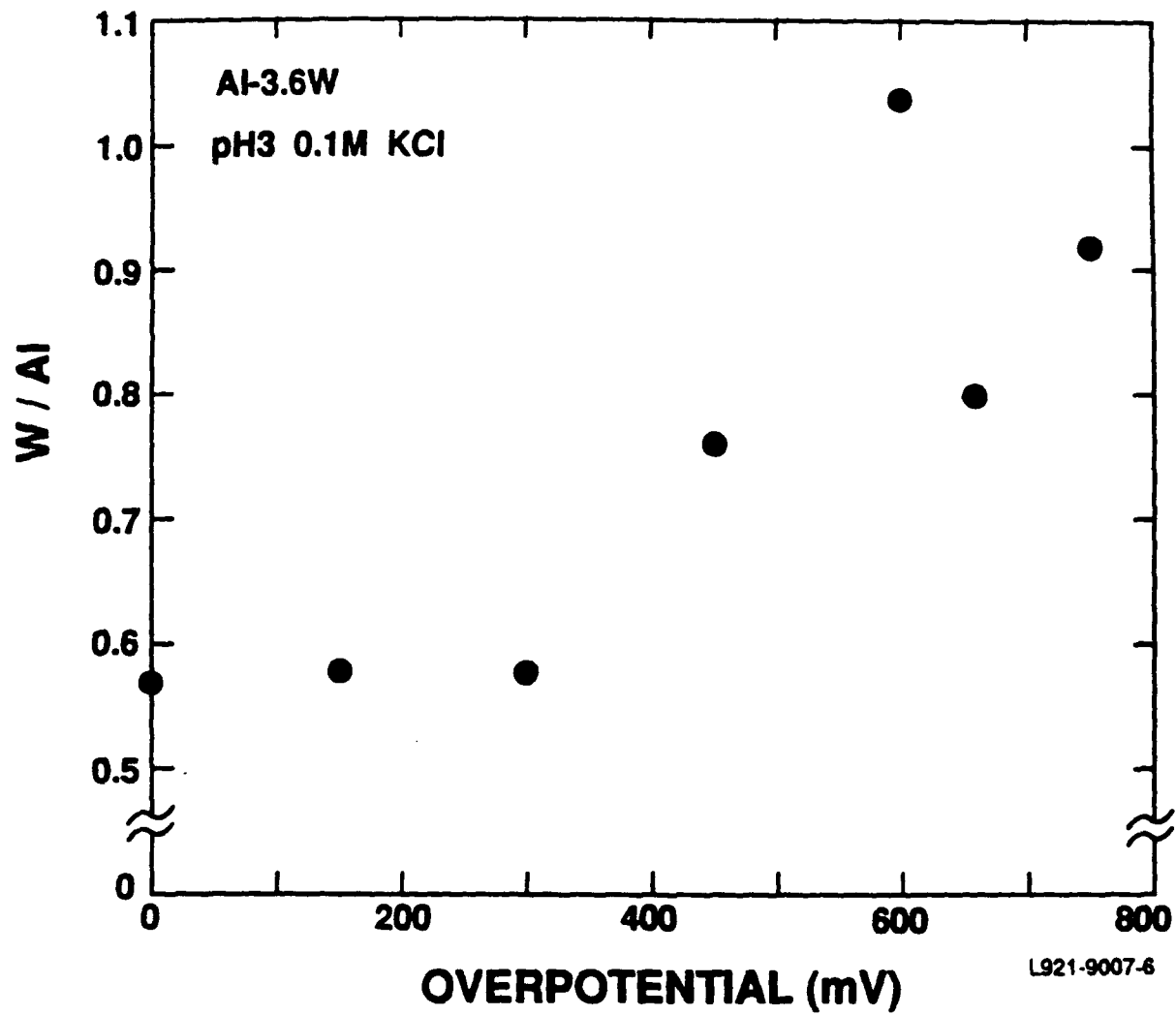
Figure 27. W/Al ratio in the passive film as a function of overpotential in a pH 3 0.1 M Cl⁻ solution.

same time. We detect only W^{+6} and W^{+4} and these states persist without chemical changes throughout the polarization sequence in approximately the same proportion. The differences may be actual chemical differences or they may reflect limitations in their energy resolution and curve fitting capabilities. In either case, at higher overpotentials, they find only W^{+6}.

Finally, Yoshioka et al. provide an independent verification of our identification of distinct elemental and alloyed W (and Mo and Cr) states as detected in samples immersed in neutral solutions where preferential oxidation of the Al leaves the interfacial region of the alloy W-rich and promotes dealloying[7]. Extrapolating from pure W and several alloy compositions, their data indicate that a W atom in an infinitely dilute Al alloy would have a 4f binding energy shift of 0.8 eV, relative to pure W, which compares very well to our measured shift of 0.7 eV for low concentration (1-10%) alloys. Similar data on their AlTa alloys show a smaller shift (~0.4 eV)[20], which is consistent with our inability to resolve an alloyed-elemental shift in our AlTa alloys.[4]

Comparison of Mechanisms

It is interesting to compare the electrochemical behavior and passive film chemistry of the various alloys we have examined with the different mechanisms put forth to explain the enhanced passivity of the nonequilibrium aluminum alloys. These mechanisms generally affect one or more of the steps involved in pitting: adsorption of Cl^-, transport of Cl^- through the passive film or stabilization of the film, and dissolution or repassivation at the passive film/metal interface. In comparing the models, it must be anticipated that different mechanisms may be simultaneously active so that the enhanced passivity could be a combined effect. Additionally, it is possible that the dominant mechanism may change depending on the alloy and the conditions of exposure/attack.

McCafferty and Natishan[12-15] have proposed that changes in the pH of zero charge, pH_{pzc}, of the passive film control pitting by affecting the adsorption of Cl^- -- the lower the pH_{pzc}, the greater the negative charge on the oxide and the less likely that Cl^- ions or any negative anion will adsorb onto the surface. They have shown good correlation plotting E_p versus pH_{pzc} of the solute oxide (Fig. 28). Of particular note is the very low pH_{pzc} of WO_3 and the high E_p of Al-W alloys. However, this correlation implicitly assumes that the passive films of the alloys consist solely of oxidized solute.

42
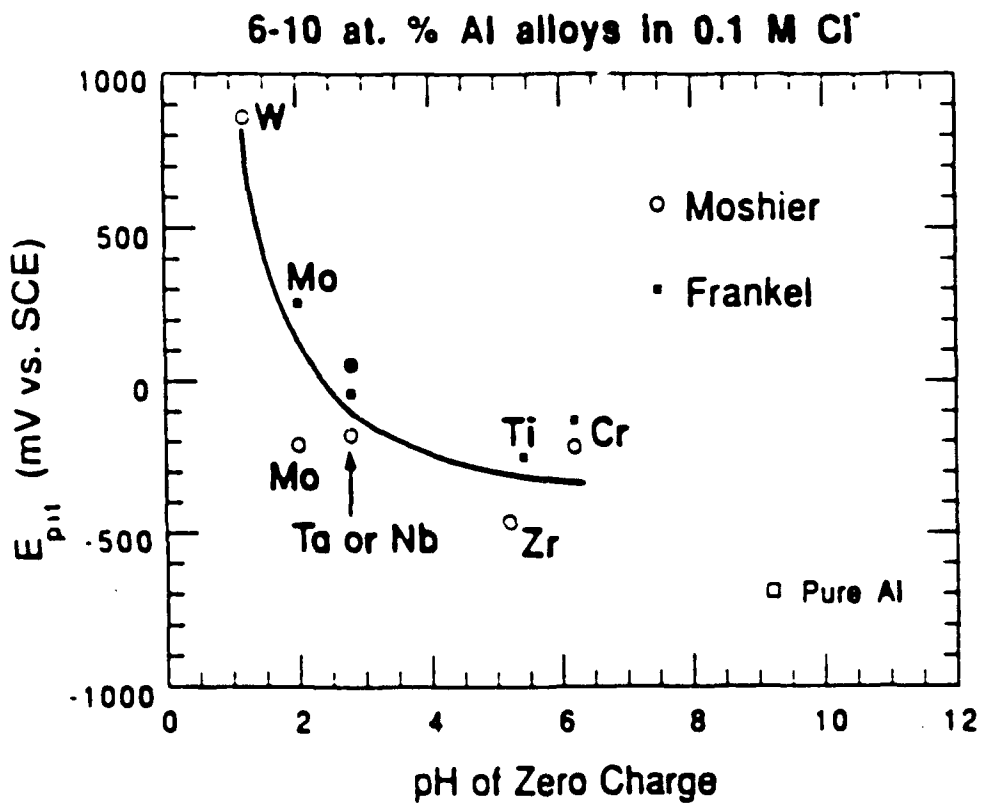
Figure 28. Pitting potentials of nonequilibrium alloys as a function of pH_{pzc} of the oxidized solute (from Reference 16).

XPS measurements show that this is not the case and that the fraction of oxidized solute varies according to alloy, alloy concentration (Al-Mo, Al-W), applied overpotential, and solution pH. It is not known how the pH_{pzc} varies with mixed oxide composition. In Parks' extensive review,[43] the only mixed oxide work reported is that of Johansen and Buchanan[44] which reported that Al_2O_3 in SiO_2 causes a shift in pH_{pzc} proportional to the molar fraction of Al_2O_3. Roy and Fuerstenau[45] later showed that small amounts of TiO_2 and MgO could cause significant shifts in the pH_{pzc} of Al_2O_3 -- 0.5-1.0%TiO_2 shifted the pH_{pzc} by -1.5 compared to a -3.6 shift for pure TiO_2 and similar amounts of MgO shifted it by 0.6 compared to a 3.4 shift for pure MgO. In both cases, there was no difference between 0.5 and 1.0% dopant. In light of the low concentration of oxidized W in the passive film (0.01-2%) near E_p in near neutral pH solutions, it is reasonable to assume that the pH_{pzc} is between that of Al_2O_3 and WO_3, but closer to that of Al_2O_3.

Figure 29 shows E_p for a variety of alloys as a function of pH_{pzc} where the pH_{pzc} was calculated from the passive film chemistry at or near E_p, assuming a linear dependence of pH_{pzc} with mixed oxide composition. Based on Roy and Fuerstenau's results, this calculation may overestimate the pH_{pzc} by an unknown amount, especially for Al-W alloys where little oxidized solute is present, but represents the only quantifiable first approximation. The figure fails to indicate any correlation between E_p and pH_{pzc} for the nonequilibrium alloys. In particular, the low concentration of oxidized W in the passive film coupled with their high E_p suggests that the pH_{pzc} mechanism alone cannot explain the enhanced passivity of this alloy unless there is a process that concentrates the oxidized W at defects or other local areas of attack. Other mechanisms must be involved. Similarly, the scatter with the other alloys suggest that pH_{pzc} considerations alone cannot explain their enhanced passivity and other mechanisms must also contribute.

The SVIM model proposed by Urguidi and Macdonald[23] is consistent with our data on Al-Mo alloys[1-3] which show an increase in E_p with increasing Mo^{+6} concentration and a decreasing Mo^{+6} concentration prior to E_p. In this case, the Mo^{+6} in the passive film is highly oxidized and could interact with cation vacancies. The electrostatic mechanism we proposed earlier[2,3] can be interpreted as a simplified version of the SVIM model. However, different mechanisms are needed to explain the passivity of Al-Cr and Al-W alloys. In Al-Cr, the Cr^{+3} has the same oxidation state as the Al^{+3} and should not interact with cation vacancies. In Al-W at near-neutral pHs, there
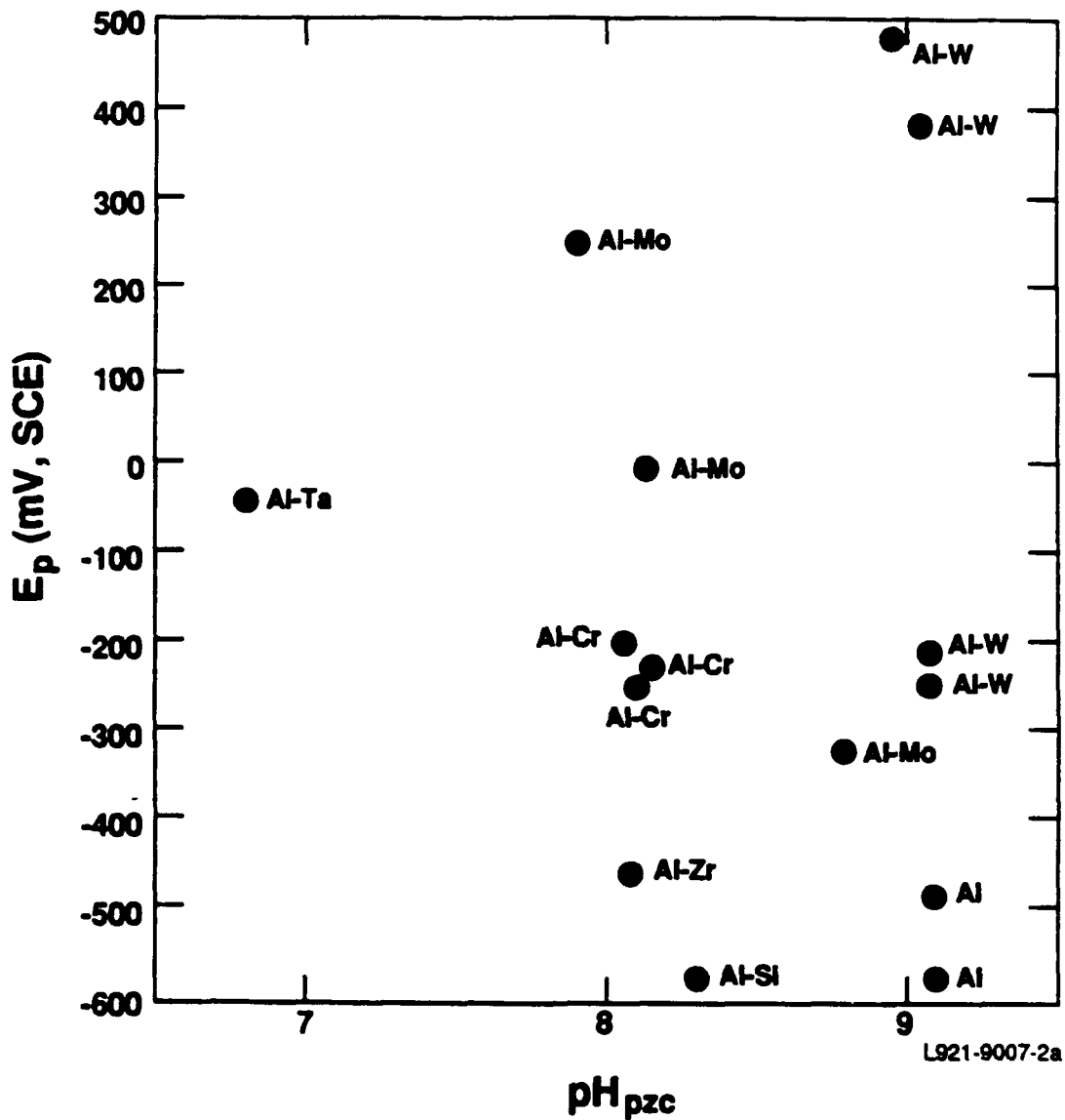
Figure 29. Pitting potentials of nonequilibrium alloys as a function of pH_{pzc} of the passive film assuming a linear relationship between the composition of a mixed oxide and the pH_{pzc} of the individual oxides.

would appear to be insufficient oxidized W to complex with the vacancies and provide the high E_p's observed.

Previously, we had speculated that small amounts of oxidized W might stabilize the passive film structure and make it less subject to attack.[7] Although this cannot be ruled out in near-neutral pH solutions, the changing passive film chemistry but similar E_p of Al-W alloys over a wide pH range suggests that structure considerations alone cannot explain the enhanced passivity. It would be difficult for a single, stable structure to persist while the passive film chemistry is changing from oxidized/hydrated Al with trace amounts of oxidized W (pH 8[7]) to comparable amounts of oxidized (pH 3) Al and W and then to oxidized W (pH 0[19]).

To explain the passivity of Al-W alloys, we need a mechanism that would allow for low oxidized W concentrations in the passive film at near-neutral pH, yet explain the passivity that is present over a wide range of pH. The establishment of a sufficiently aggressive solution within preexisting defects at the passive film/metal interface and the resulting active dissolution of the metal have been proposed as the rate-determining steps for the breakdown of passivity. Metastable pits in these corrosion-resistant nonequilibrium alloys form when the metal dissolution rate within the pits is too low to sustain a sufficiently low pH and repassivation occurs.[21,22] This mechanism assumes the presence of preexisting flaws extending to the substrate/oxide interface. It has also been speculated that the flaws are primarily located over grain boundaries in the underlying metal.[21,22] As the volume fraction of the grain boundary region increases (with smaller grains), the passive film, especially an epitaxial monolayer at the interface, exhibits a larger number of uniformly distributed defects at the grain boundaries. These defects reportedly provide a high degree of competition for available Cl⁻ anions so that localized enrichment of Cl⁻ and subsequent acidification require a greater driving force and, hence, a higher potential for stable pit growth. If the concentration of such defects control passivity, then one would expect a correlation of E_p with grain size and amorphous alloys should exhibit higher pitting potentials than crystalline alloys with similar solute concentration. A compilation of available grain size versus E_p data (Fig. 15) shows little correlation over the entire range of grain size. Furthermore, comparison of the pitting potentials for different W compositions and crystallity in Fig. 30 shows that amorphous and crystalline specimens with the same composition exhibit identical pitting potentials. Since the passive films of these aluminum alloys are amorphous regardless of the crystallinity of

46
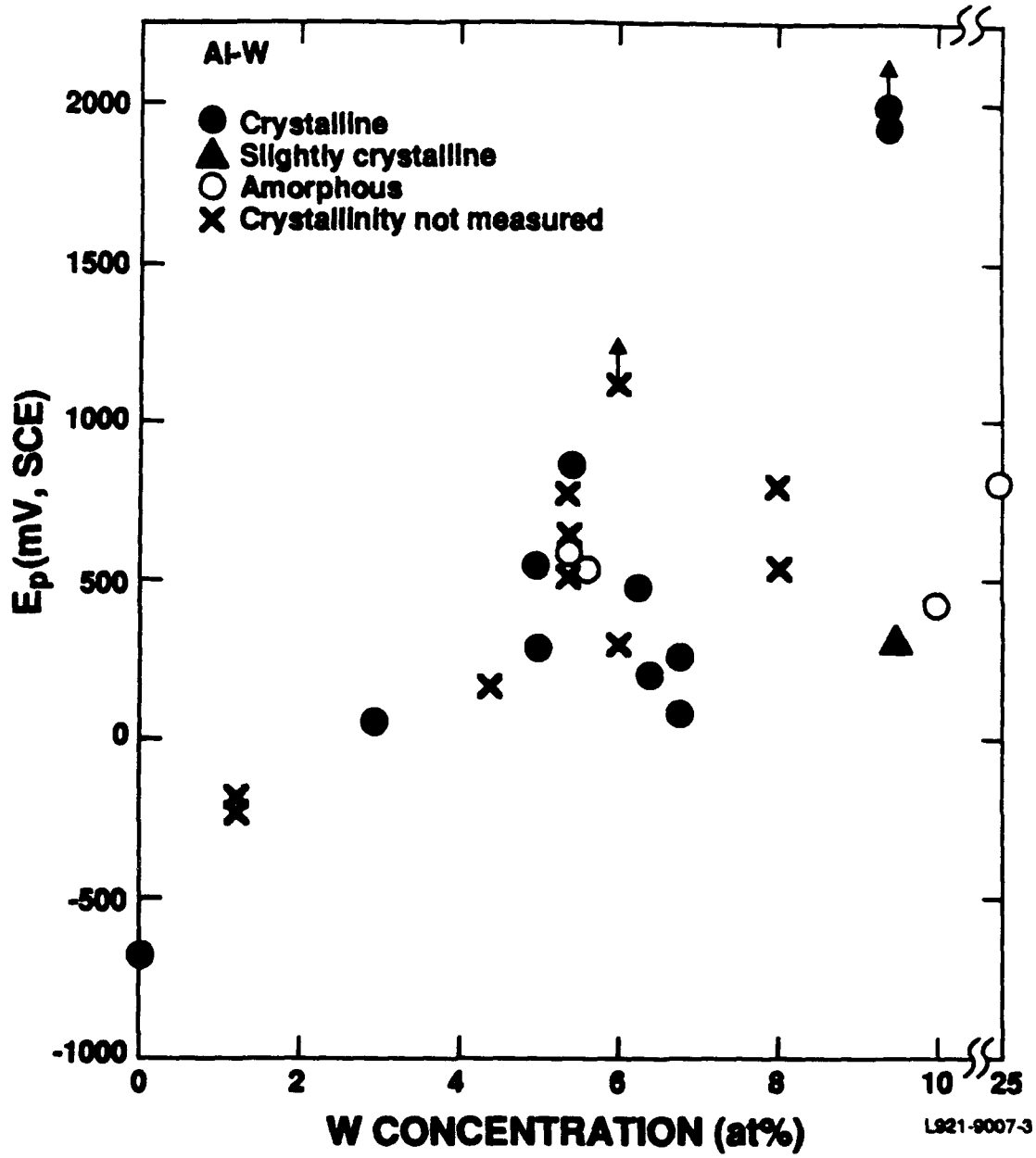
Figure 30. Pitting potential of AlW alloys as a function of W concentration. Crystallinity, as determined by XRD or SAD, is noted when known.

47

the substrate (with the possible exception of an epitaxial monolayer of oxide), the composition of the film (or composition-induced local structural changes) appears to be a greater factor influencing passivity.

A version of this mechanism could explain passivity despite the low average concentration of oxidized W. Once a defect is formed at the passive film/metal interface and dissolution/acidification begins, an oxidized W film grows locally as the Al dissolves. This oxidized W is more stable than the original film at low pH and passivates the site. Additional passivity may occur since, according to the pH_{pzc} model, less Cl⁻ would adsorb locally. Although the average concentration of W in the passive film may be low at near-neutral pH, it could be high in passivated pits. If this were the case, one would expect its average concentration to increase with anodic overpotentials as the concentration of passivated pits increases. We do indeed observe this increase in oxidized W during polarization.[7] During polarization in the pH 3 solutions, the local environment in a metastable pit is partially simulated over the entire specimen and high oxidized W concentrations are seen.

SUMMARY AND CONCLUSIONS:

We were unsuccessful in producing rapidly solidified single-phase Al-W and Al-Ta powders; precipitates were present in all.

Dynamic compaction of Al-Ta powders and of Al-W powders with water did not lead to the formation of new precipitates or to substantial growth of existing ones. Compaction of Al-W powders with air did affect precipitation, resulting in the disappearance of an unidentified phase and nucleation of WAl_{12}.

The precipitates in the compacted material formed microgalvanic cells and led to pitting. No enhanced passivity was observed.

Nonequilibrium, single-phase Al-W alloys exhibited enhanced passivity over a wide range of pH (0-9.6) and Cl⁻ concentration (0.1-1.0 M), including artifical seawater. The pitting potential was nearly constant over this range, with an apparent slight maximum at pH 8. The passive current density showed a strong dependence on pH, increasing with decreasing pH.

The Al-Ta alloys exhibited enhanced passivity at high pH values and some evidence of passivity at low pH values.

The passive film of Al-W alloys in pH 3 solutions is thicker that that observed in near-neutral solutions and contains more than two orders of magnitude more oxidized W. Because of a composition gradient in the film at E_{oc}, the surface was more W-rich than the substrate side. As an anodic potential was applied, the passive film became more W-rich up to the pitting potential.

The excellent corrosion behavior of Al-W alloys over a wide range of pH coupled with the low W concentration in the passive film formed at near-neutral pH suggest a different mechanism is involved than for other "stainless" aluminum alloys. Many of the proposed passivity mechanisms, such as barrier layer formation, vacancy-solute complex formation, pH_{pzc}, structure stabilization, and grain boundary defect-competition are not consistent with the Al-W results.

The most likely mechanism to explain the passivity of Al-W alloy involves the local passivation of a metastable pit due to the stability of the oxidized solute in low pH conditions.

Acknowledgements

REFERENCES

1. W.C. Moshier, G.D. Davis, J.S. Ahearn, and H.F. Hough, J. Electrochem. Soc. **133**, 1063 (1986).
2. W.C. Moshier, G.D. Davis, J.S. Ahearn, and H.F. Hough, J. Electrochem. Soc. **134**, 2677 (1987).
3. W.C. Moshier, G.D. Davis, and G.O. Cote, J. Electrochem. Soc. **136**, 356 (1989).
4. G.D. Davis, W.C. Moshier, T.L. Fritz, and G.O. Cote, J. Electrochem. Soc. **137**, 422 (1990).
5. B.A. Shaw, T.L. Fritz, G.D. Davis, and W.C. Moshier, J. Electrochem. Soc. **137**, 1317 (1990).

6. G.D. Davis, W.C. Moshier, G.G. Long, and D.R. Black, J. Electrochem. Soc. **138**, 3194 (1991).
7. B.A. Shaw, G.D. Davis, T.L. Fritz, B.J. Rees, and W.C. Moshier, J. Electrochem. Soc. **138**, 3288 (1991).
8. B.A. Shaw, G.D. Davis, T.L. Fritz, B.J. Rees, and W.C. Moshier, in *Critical Factors in Localized Corrosion*, G.S. Frankel and R.C. Newman, eds. (The Electrochemical Society, Pennington, NJ, in press).
9. G.S. Frankel, M.A. Russak, C.V. Jahnes, M. Mirzamaani, and V.A. Brusic, J. Electrochem. Soc. **136**, 1243 (1989).
10. A.H. Al-Saffar, V. Ashworth, A.K.O. Vairamov, D.J. Chivers, W.A. Grant, R.P.M. Procter, Corros. Sci. **20**, 127 (1980).
11. M.V. Zeller and J.A. Kargol, Appl. Surf. Sci. **18**, 63 (1984).
12. P.M. Natishan, E. McCafferty, and G.K. Hubler, J. Electrochem. Soc. **133**, 106¹ (1986).
13. E. McCafferty, G.K. Hubler, P.M. Natishan, P.G. Moore, R.A. Kant, and B.D. Sartwell, Mater. Sci. Eng. **86**, 1 (1987).
14. P.M. Natishan, E. McCafferty, and G.K. Hubler, J. Electrochem. Soc. **135**, 321 (1988).
15. P.M. Natishen, E. McCafferty, and G.K. Hubler, Corros. Sci. **32,** 721 (1991).
16. E. McCafferty and P.M. Natishan, in *Critical Factors in Localized Corrosion*, G.S. Frankel and R.C. Newman eds. (The Electrochemical Society, Pennington, NJ, in press).
17. R.W. Gardiner and M.C. McConnell, Met. Mater. **3**, 254 (1987)
18. M. Fass, D. Itzhak, D. Eliezer, F.H. Froes, J. Mater. Sci. Lett. **6**, 1227 (1987).
19. H. Yoshioka, H. Habazaki, A. Kawashima, K. Asami, and K. Hashimoto, Corros. Sci. **32**, 313 (1991).
20. H. Yoshioka, A. Kawashima, K. Asami, and K. Hashimoto, in *Proc. Symp. Corrosion, Electrochmistry, and Catalysis of Metallic Glasses* R.B. Diegle and K. Hashimoto, eds. (The Electrochemical Society, Pennington, NJ 1988) p. 242.
21. R.B. Inturi and Z. Szklarska-Smialowska, submitted to J. Electrochem. Soc.
22. Z. Szklarska-Smialowska, in *Critical Factors in Localized Corrosion*, G.S. Frankel and T.C. Newman, eds. (The Electrochemical Society, Pennington, NJ, in press).
23. M. Urguidi and D.D. Macdonald, J. Electrochem. Soc. **132**, 555 (1985)
24. M. Pourbaix, *Atlas of Electrochemical Equilibria in Aqueous Solutions*, (NACE, Houston, TX 1974) p. 168.
25. N. Bui, A. Irhzo, F. Dabosi, and Y. Limouzin-Maire, Corros. **39**, 491 (1983).
26. A. Irhzo, Y. Segui, N. Bui, and F. Dabosi, Corros. Sci. **26**, 769 (1986).
27. H. Habazaki. A. Kawashima, Kasami, and K. Hashimoto, in *The Applications of Surface Analysis Methods to Environmental/Material Interactions* (PV 91-7) D.R. Baer, C.R. Clayton, and G.D. Davis, eds., (The Electrochemical Society, Pennington, NJ, 1991) p. 467.
28. J. Chen and J.K. Wu, Corros. Sci. **30**, 53 (1990).
29. G.D. Davis, T.L. Fritz, B.J. Rees, B.A. Shaw, and W.C. Moshier, "A study of the influence of alloying additions on the passivity of aluminum," MML TR 91-10c, Annual report submitted to ONR, March 1991.
30. R.N. Wright, G.E. Korth, and J.E. Flinn, Advanced Materials and Processes **10,** 56 (1987).
31. J.E. Flynn, G.E. Korth, R.N. Wright, and R.C. Green, in *Shock Waves in Condensed Matter*, Y.M. Gupta ed., (Plenum, New York, 1986), p. 713.

32. M. Nathan, Mater. Lett. **3**, 319 (1985).
33. G.D. Davis, W.C. Moshier, J.S. Ahearn, H.F. Hough and G.O. Cote, J. Vac. Sci. Technol. A **5**, 1152 (1987).
34. C.D. Wagner and D.M. Bickham, NIST Standard Reference Database 20, NIST X-ray Photoelectron Spectroscopy Database, Version 1.0, NIST, Gaithersburg, MD (1989).
35. C.D. Wagner, W.M. Riggs, L.E. Davis, J.F. Moulder, and G.E. Muilenberg, eds., *Handbook of X-ray Photoelectron Spectroscopy* (Perkin-Elmer, Eden Praire, MN 1979).
36. C.D. Wagner, in *Practical Surface Analysis*, D. Briggs and M.P Seah, eds., (Wiley, Chichester 1983) p. 477.
37. G.E. McGuire, G.K. Schweitzer, and T.A. Carlson, Inorg. Chem. **12**, 2450 (1973).
38. K.T. Ng and D.M. Hercules, J. Phys. Chem. **80**, 2094 (1976).
39. R.J. Colton and J.W. Rabalais, Inorg. Chem. **15**, 236 (1976).
40. P. Biloen, and G.T. Pott, J. Catal. **30**, 169 (1973).
41. J.F. Morar, F.J. Himpsel, G. Hughes, J.L. Jordon, F.R. McFeely, and G. Hollinger, J. Vac. Sci. Technol. A **3**, 1477 (1985).
42. B.S. Shaw and W.C. Moshier, unpublished results.
43. G.A. Parks, Chem. Rev. **65**, 177 (1965)
44. P.G. Johansen and A.S. Buchanan, Aust. J. Chem. **10**, 398 (1957).
45. P. Roy and D.W. Fuerstenau, Surf. Sci. **30**, 487 (1972).